

DETERMINING THE MAXIMUM POWER TRANSFER CAPACITY OF SPUR GEARS MOUNTED ON SHAFTS WITH SPLINE BUSHES

William Manjud Maluf Filho

Fatec Diadema, Industrial Production
Management Technology professor, Diadema
– SP, Brazil
<https://lattes.cnpq.br/9888914170875821>

Alexandre Barbosa de Melo

Fatec Diadema, Industrial Production
Management Technology student, Diadema –
SP, Brazil
[https://www.linkedin.com/in/alexandre-
barbosa-59b7911a8](https://www.linkedin.com/in/alexandre-barbosa-59b7911a8)

Carlos Eduardo Vieira Silva

Fatec Diadema, Industrial Production
Management Technology, Diadema – SP,
Brazil

João Felipe de Souza Lourenço

Centro Universitário FEI, Mechanical
Engineering student, São Bernardo do
Campo – SP, Brazil
[https://www.linkedin.com/in/jo%C3%A3o-
felipe-de-souza-louren%C3%A7o-72a3a0139](https://www.linkedin.com/in/jo%C3%A3o-felipe-de-souza-louren%C3%A7o-72a3a0139)

Victor Michael da Silva

Fatec Diadema, Industrial Production
Management Technology, Diadema – SP,
Brazil
[https://www.linkedin.com/in/victor-michael-
25a972249](https://www.linkedin.com/in/victor-michael-25a972249)

All content in this magazine is licensed under a Creative Commons Attribution License. Attribution-Non-Commercial-Non-Derivatives 4.0 International (CC BY-NC-ND 4.0).



Abstract: This technical article focuses on determining the maximum power transfer capacity of spur gears mounted on shafts with spline bushes using an interference fit. Spur gears play a crucial role in power transmission systems, and the use of spline bushes with an interference fit provides enhanced stability, load distribution, and safety. The gear is mounted on the spline bush, which, in turn, is mounted on the shaft using interference fit. This arrangement ensures that in case of torque overload, the interference fit allows the spline bush to slip preventing mechanical structural failure of the transmission elements. Understanding the maximum power capacity of these gear systems is essential for ensuring reliable and efficient operation. The article provides an overview of spur gears, spline bushes, and the benefits of an interference fit. It explores the factors influencing power transmission and presents analytical methods for calculating critical parameters. A case study calculation is included to demonstrate the application of the discussed methods. Design considerations and optimization techniques for enhancing power capacity are also discussed. By determining the maximum power transfer capacity, engineers can make informed design decisions, optimize gear systems, and ensure both reliable power transmission and safety.

Keywords: Spur gears; Spline bushes; Interference fit; Power transmission; Maximum power capacity.

INTRODUCTION

In power transmission systems, spur gears play a pivotal role in efficiently transmitting torque and rotational motion. The reliable and optimal performance of these gears is crucial for various industrial applications such as automotive, machinery, and robotics. One key aspect of ensuring their reliable operation is determining the maximum power transfer

capacity, which is essential for designing gear systems that can handle the intended load without failure.

In recent years, the use of spline bushes with an interference fit has gained significant attention in the field of gear system design. Spline bushes serve as a mounting interface between the gear and the shaft, providing stability and load distribution. The interference fit, achieved through a controlled amount of interference between the spline bush and the shaft, enhances the connection strength and eliminates any potential play or backlash.

However, the use of an interference fit in spline bushes offers more than just a rigid connection. It introduces a safety aspect to the gear system. In the event of a torque overload or sudden shock load, the interference fit allows the spline bush to slip on the shaft, effectively absorbing the excess load and preventing mechanical structural failure of the transmission elements. This safety mechanism adds an extra layer of protection and reliability to the gear system.

The primary objective of this technical article is to determine the maximum power transfer capacity of spur gears mounted on shafts with spline bushes using an interference fit. By accurately calculating the maximum power capacity, engineers can make informed design decisions and optimize gear systems to ensure reliable and efficient operation while considering safety aspects.

This article provides an overview of spur gears, spline bushes, and the benefits of utilizing an interference fit in their design. It explores the factors that influence power transmission in such gear systems, including tooth strength, contact stress, and bending fatigue. Analytical methods and calculations for determining critical parameters will be presented, along with a practical case study to illustrate their application.

Furthermore, design considerations and

optimization techniques for enhancing power capacity will be discussed, enabling engineers to refine gear system designs and maximize performance. By understanding and optimizing the maximum power transfer capacity, engineers can develop gear systems that meet the required load demands while ensuring long-term reliability and safety.

This article has the following sections.

a) Introduction: briefly introduce the concept of spur gears mounted on shafts with spline bushes and their significance in power transmission systems. State the objective of the article: to determine the maximum power transfer capacity of such gear systems.

b) Overview Of Mechanical Power Transmission Elements: explain key reasons why power transmission through mechanical elements is vital. Provide a general explanation of the most common mechanical components used to transmit power.

c) Overview of Spur Gears and Spline Bushes: provide a general explanation of spur gears, their functionality, and common applications. Explain the purpose and role of spline bushes in gear mounting and power transmission. Discuss the advantages of using an interference fit for mounting the spline bush on the shaft.

d) Power Transmission Considerations: explain the factors influencing power transmission in spur gear systems. Discuss key considerations such as gear material, tooth design, lubrication, and efficiency. Highlight the importance of calculating the maximum power capacity to ensure reliable and efficient operation.

e) Analysis of Interference Fit in Spline Bushes: explain the concept of interference fit and its role in enhancing

power transmission capability. Discuss the benefits and challenges associated with interference fit in spline bush mounting. Present equations and methodologies for calculating the interference fit parameters.

f) Determining the Maximum Power Transfer Capacity: describe the approach for determining the maximum power transfer capacity of the gear system. Discuss the critical factors affecting power capacity, including tooth strength, contact stress, and bending fatigue. Present analytical methods, such as AGMA standards or FEA (Finite Element Analysis), for calculating these factors.

g) Case Study: present a practical case study or example calculation to illustrate the application of the methods discussed. Walk through the calculation step-by-step, highlighting the key parameters and assumptions. Provide a clear conclusion regarding the maximum power transfer capacity achieved in the case study.

h) Design Considerations and Optimization Techniques: discuss design considerations for enhancing the power capacity of spur gear systems with spline bushes. Explore optimization techniques such as tooth profile modification, material selection, and lubrication improvements. Highlight the importance of iterative design and testing to validate the calculated power capacity.

i) Conclusion: summarize the key points discussed in the article. Emphasize the significance of determining the maximum power transfer capacity for reliable and efficient gear system design. Mention potential future advancements and research areas in this field.

j) Acknowledgments: express gratitude

and acknowledge individuals or organizations that have contributed to the development of the technical article

k) References: list all the sources you have cited throughout the article. This includes books, research papers, journal articles, conference proceedings, websites, and any other relevant publications. The references are properly formatted according to NBR 6023/2018 and allow readers to explore the sources for further information or verification.

l) Appendix A: the main author of this article, a professor at the Mechanical Engineering College, has extensive expertise in the field of machine design and has created a comprehensive summary of the main mathematical expressions utilized in the analysis of interference fit and spline shafts. So the appendix is dedicated to providing supplementary material that complements the main content of the article. This additional material serves as a valuable resource for readers who may be interested in further understanding the concepts or applying them in practical scenarios.

m) Appendix B: in order to facilitate the practical implementation of the methods discussed in this article, a set of Excel sheets has been prepared to assist in the case study calculations. These Excel sheets serve as valuable tools for engineers and researchers involved in gear system design and analysis. The Excel sheets are designed to provide a user-friendly interface where the necessary input parameters can be entered, and the calculations for determining the maximum power transfer capacity can be performed automatically. They incorporate the equations and methodologies presented

in Section 7 (Case Study) to ensure accuracy and reliability.

In traditional technical articles, the literature review is typically presented in a dedicated section, providing a comprehensive overview of existing research and knowledge. However, in this article, the authors have chosen a different approach. Instead of confining the literature review to a single section, it is incorporated throughout the various sections, closely accompanying the specific topics discussed. This decision was made to ensure that the relevant literature is seamlessly integrated into each corresponding subject, offering a more coherent and contextual understanding of the topic at hand. By deploying the literature review in this manner, readers are provided with a continuous flow of information and a deeper appreciation of the significance of previous research within the specific contexts addressed.

The literature review for this article was meticulously conducted by consulting renowned scientific databases and authoritative reference books. Noteworthy scientific databases, such as IEEE Xplore, ScienceDirect, and ACM Digital Library, were utilized to access a wide range of scholarly articles, conference papers, and technical reports. These databases served as invaluable resources for gathering up-to-date information, comprehensive studies, and cutting-edge advancements in the field of gear systems, interference fit, and power transmission. Furthermore, reference books authored by subject matter experts provided additional insights, historical perspectives, and foundational knowledge, contributing to a well-rounded literature review.

In the process of conducting the literature review and preparing this technical article, artificial intelligence tools played a pivotal role. AI tools were employed to identify

relevant literature, perform efficient searches within the selected databases, and sort the obtained references based on relevance and significance. These intelligent tools leveraged advanced algorithms and machine learning techniques to streamline the research process, enabling the authors to access a vast pool of information quickly and effectively. Moreover, AI tools were utilized to assist in the writing process, aiding in the organization of ideas, data synthesis, and overall article structure. By harnessing the power of artificial intelligence, the authors were able to enhance the efficiency and quality of the article, ultimately providing a more comprehensive and valuable resource for readers.

In summary, determining the maximum power transfer capacity of spur gears mounted on shafts with spline bushes using an interference fit is essential for designing robust and efficient gear systems. This article aims to provide insights into the calculations, considerations, and optimizations required to achieve optimal power transmission while maintaining the safety and reliability of the system.

OVERVIEW OF MECHANICAL POWER TRANSMISSION ELEMENTS

Transmitting power using mechanical elements is of utmost importance in various industries and applications. Mechanical power transmission allows for the controlled and efficient transfer of energy from one component to another, enabling the functioning of machinery, equipment, and systems. An example of mechanical elements applied to transmit power is shown in Figure 1.

Here are several key reasons why power transmission through mechanical elements is vital:

a) Efficiency: mechanical power

transmission systems are designed to minimize energy losses and maximize efficiency. By employing mechanical elements that are properly sized, lubricated, and aligned, energy can be transmitted with minimal losses, resulting in optimized performance and reduced energy consumption (DING *et al.*, 2022).

b) Control: mechanical power transmission offers precise control over the speed, torque, and direction of power transfer. By selecting appropriate mechanical elements, such as gears, belts, or chains, engineers can tailor the power transmission characteristics to meet specific operational requirements and maintain control over the machinery or system (KUMAR *et al.*, 2022).

c) Reliability: mechanical power transmission systems are known for their robustness and reliability. Mechanical elements are designed to withstand high loads, shocks, and vibrations commonly encountered in industrial applications. By employing reliable mechanical components, the risk of power loss, system failure, and downtime can be significantly reduced, ensuring uninterrupted operation (JIANG *et al.*, 2023a).

d) Versatility: mechanical power transmission offers versatility in terms of the range of applications it can serve. Mechanical elements can be combined and configured in various ways to accommodate different power requirements, distances, and environmental conditions. This flexibility allows for the design and implementation of power transmission systems across a wide array of industries and machinery (DUDEK *et al.*, 2023).

e) Maintenance and serviceability: mechanical power transmission systems are typically easier to maintain and service compared to other forms of power transmission. Mechanical components can be inspected, lubricated, and replaced as needed, facilitating routine maintenance and reducing downtime. Furthermore, troubleshooting and repair of mechanical elements can often be performed without the need for specialized equipment or expertise (GRAZIOSO *et al.*, 2019).

The main mechanical elements used in power transmission include:

a) Gears: spur gears, helical gears, bevel gears, and worm gears are commonly used to transmit power and motion between rotating shafts. They are versatile and can achieve different speed ratios, torque multiplication, and direction changes (MU *et al.*, 2023).

b) Belts and pulleys: belt drives are prevalent in many applications, utilizing flexible belts and pulleys to transfer power. They offer smooth operation, adaptability to various distances, and are ideal for situations where vibration and noise reduction are important (ISLAM *et al.*, 2022).

c) Chains and sprockets: chain drives consist of interconnected links and sprockets that transmit power. They are known for their high strength and ability to handle heavy loads, making them suitable for demanding industrial environments (VOINA *et al.*, 2022).

d) Shafts and couplings: shafts are mechanical elements used to connect rotating components and transmit torque. Couplings are used to join shafts together, allowing for the transmission of power while compensating for

misalignment and absorbing shock and vibration (JIANG *et al.*, 2023b).

e) Bearings: bearings are essential for reducing friction and supporting rotating shafts. They enable smooth operation and help maintain the alignment and stability of rotating components (REJITH *et al.*, 2023).

These mechanical elements, among others, form the building blocks of power transmission systems and are crucial for effective and reliable energy transfer in industrial settings (PALERMO *et al.*, 2018).

OVERVIEW OF SPUR GEARS AND SPLINE BUSHES

In this chapter we provide a general explanation of spur gears and spline bushes. We explore their functionality, common applications and we explain the purpose and role of in gear mounting and power transmission systems.

SPUR GEARS

Spur gears are one of the most common and widely used types of gears in mechanical power transmission systems. They are renowned for their simplicity, efficiency, and versatility. Spur gears consist of cylindrical teeth that are parallel to the gear axis and mesh with other gears to transmit power and motion (CHANG *et al.*, 2023).

There are some key features and design considerations such as:

a) Gear teeth: spur gears have straight, parallel teeth that extend radially from the gear's circumference. The shape and profile of the gear teeth play a crucial role in determining the efficiency, load capacity, and noise level of the gear system (MELCONIAN, 2019).

b) Gear ratio: the gear ratio of a spur gear system is determined by the number of

teeth on the mating gears. It represents the relationship between the rotational speed and torque between the driver and driven gears (BHANDARI, 2010).

c) Tooth engagement: spur gears engage in a rolling contact, where the gear teeth mesh and transfer power by maintaining contact along the line of action (HUSSEIN; ABDULLAH, 2022). Proper tooth engagement and alignment are essential for efficient power transmission and minimizing wear (JUVINALL; MARSHEK, 2019).

d) Gear materials: spur gears are commonly made from various materials, including steel, cast iron, and non-metallic materials such as plastics or composites. The choice of gear material depends on factors such as load capacity, operating conditions, and cost considerations (RAEYMAEKERS, 2022).

e) Lubrication: proper lubrication is crucial for reducing friction, wear, and noise in spur gear systems. Lubricants such as oils or greases are applied to the gear teeth to ensure smooth operation and prevent excessive heat generation (PARMLEY, 2000).

f) Gear design and analysis: the design process for spur gears involves considerations such as tooth profile, module or pitch, pressure angle, backlash, and clearance. Advanced design tools, such as computer-aided design (CAD) software and gear design standards, aid in creating efficient and reliable gear systems (JADON; VERMA, 2014).

Spur gears find extensive use in various industries and applications, including:

a) Automotive: spur gears are employed in vehicle transmissions, differential systems, and steering mechanisms (NAUNHEIMER *et al.*, 2011).

b) Industrial machinery: they are used in power generation equipment, conveyors, machine tools, and printing presses (YAO *et al.*, 2021).

c) Robotics: spur gears are utilized in robot joints, manipulators, and precision motion control systems (NENTWICH; DAUB, 2022).

d) Home appliances: they can be found in appliances like washing machines, kitchen mixers, and power tools (GUPTA; JAIN, 2014).

e) Aerospace and Defense: spur gears are employed in aircraft landing gear systems, missile guidance mechanisms, and navigation equipment (ZHU *et al.*, 2020).

Spur gears offer numerous advantages, including simplicity, high efficiency, and the ability to transmit high loads. However, they can produce noise and vibration due to the direct contact between gear teeth. An example of a Computer Fluid Dynamics (CFD) analysis performed in meshed spur gears is shown in Figure 2.

Proper design, lubrication, and maintenance practices help mitigate these issues and ensure optimal performance (COLLINS *et al.*, 2009). The nomenclature of gear teeth is shown in Figure 3.

SPLINE BUSH

A plain bush, also known as a plain bearing or a plain sleeve bushing, is a cylindrical component with a smooth inner and outer surface. It is typically used to provide support and reduce friction between rotating or sliding components. Plain bushes are commonly made of materials such as bronze, brass, or self-lubricating polymers (CUI *et al.*, 2023). An example of plain bush is shown in Figure 4.

On the other hand, a spline bush, or spline

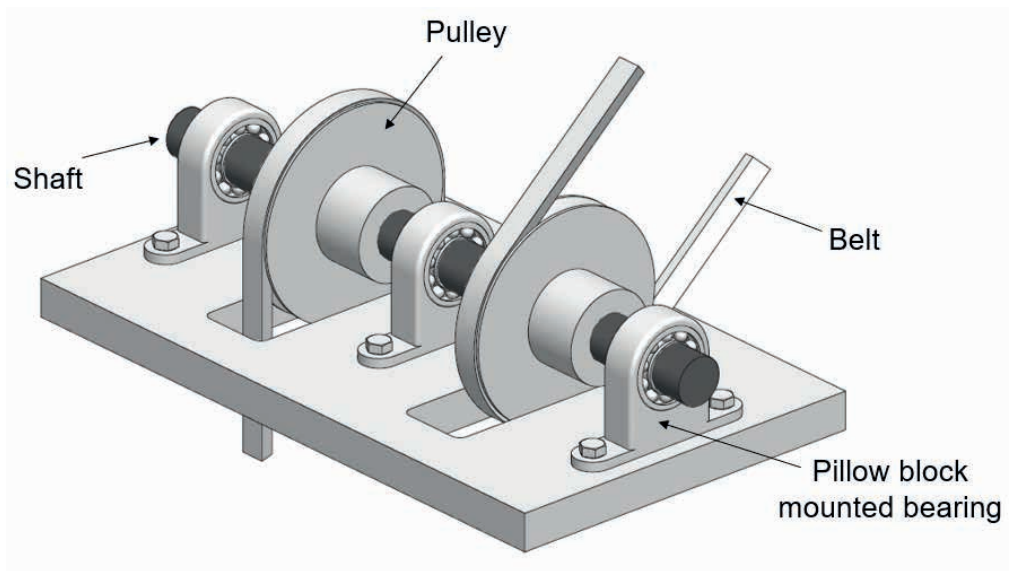


Figure 1 - Power transmitting mechanical system (adapted from SKAKOON, 2008)

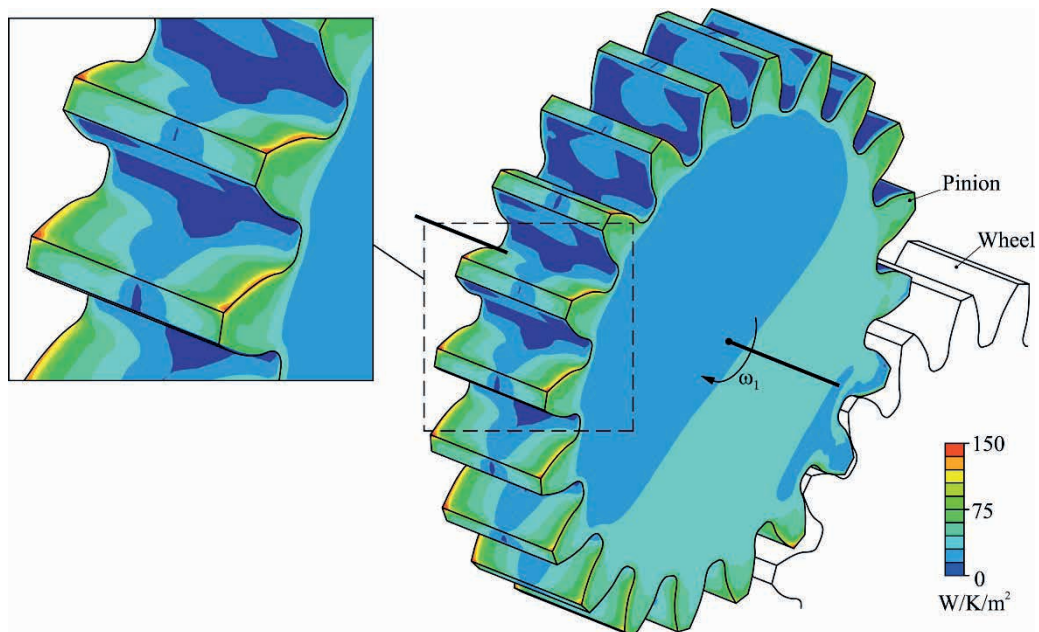


Figure 2 - Contour plot of the local heat transfer coefficient obtained from the CFD analysis of a spur gear transmission (RODA-CASANOVA *et al.*, 2023)

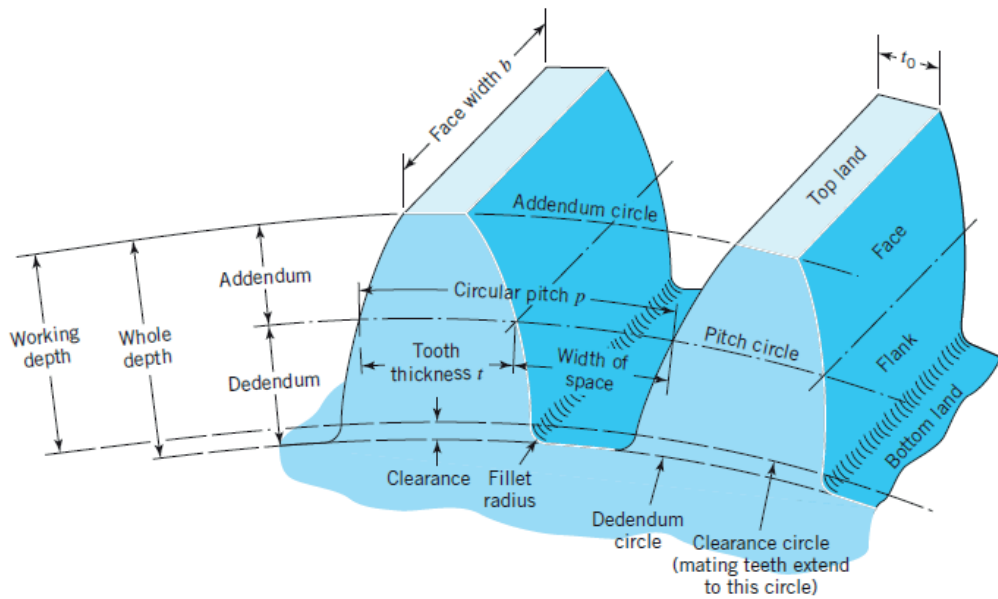


Figure 3 - Nomenclature of gear teeth (JUVINALL; MARSHEK, 2019)

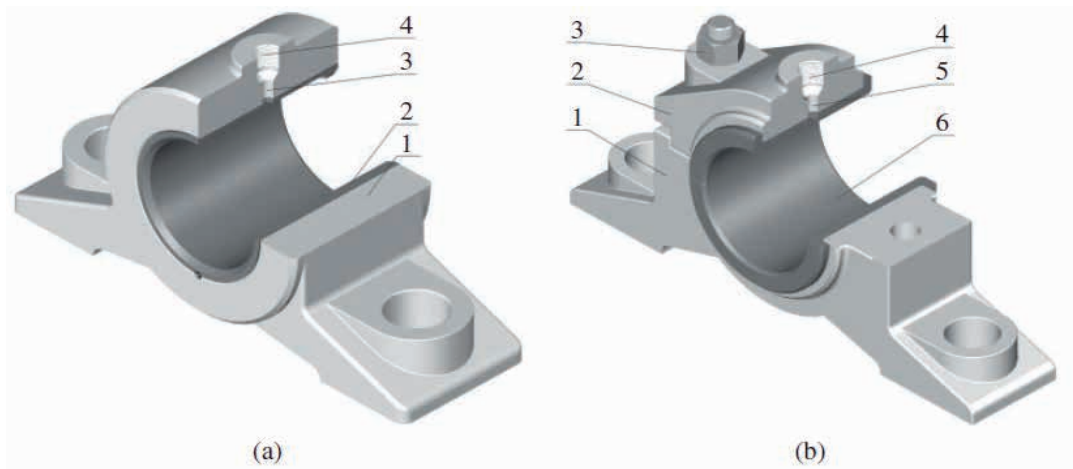


Figure 4 - Structures of sliding bearings: (a) 1 housing, 2 bushing, 3 oil hole and 4 screw; (b) 1 housing, 2 housing cover, 3 stud, 4 screw, 5 oil hole and 6 liner or bushing (JIANG, 2019)



Figure 5 - Spline bushing for 1:5 tapered shaft (<https://www.hydraspecma.com/store/dk/en/find/item/10503>)

bearing, is a specialized type of bushing designed to engage with a corresponding spline on a mating component, such as a gear or a shaft. Spline bushes are used to transmit torque, ensure accurate alignment, and resist axial and radial movement (ZHANG *et al.*, 2023). An example of a spline bushing for a tapered shaft is shown in Figure 5.

Spline bushes play a crucial role in power transmission systems, particularly in connecting gears to shafts. They provide stability, load distribution, and precise alignment, ensuring efficient power transfer and reliable operation. Spline bushes are commonly used in various industries, including automotive, aerospace, industrial machinery, and more (REGIS *et al.*, 2023).

There are some key features and design considerations, including:

a) Types of splines: there are different types of splines used in spline bushes, such as involute splines, straight-sided splines, and serrations. Each type has its own advantages and design considerations based on the specific application requirements (YAGHOUBI; TAVAKOLI, 2022).

b) Interference fit: spline bushes are mounted on shafts using an interference fit. This means that the inner diameter of the bush is slightly smaller than the outer diameter of the shaft, creating a tight fit when assembled. The interference fit provides a secure and rigid connection, preventing slippage during operation (CHEN; YANG, 2023).

c) Load distribution: spline bushes help distribute the load evenly along the shaft, minimizing stress concentrations and enhancing the overall strength of the power transmission system. They provide support and reduce the risk of localized wear or failure (BAUMANN *et al.*, 2022).

d) Alignment and tolerance: proper alignment and tolerance are critical in spline bush design. Precise machining and fitting ensure accurate positioning of the spline bush on the shaft, enabling smooth and efficient power transfer. Tolerance considerations include clearance, backlash, and fit types (such as clearance fit, transition fit, or interference fit) (DUNCHEVA *et al.*, 2022).

e) Material selection: spline bushes are typically made from materials with excellent strength, wear resistance, and dimensional stability. Common materials include alloy steels, stainless steels, and engineering plastics. The choice of material depends on factors such as load capacity, operating conditions, and compatibility with other system components (WOLLMANN *et al.*, 2022).

There are some advantages and applications, including:

f) Load transmission: spline bushes efficiently transmit torque and power from the gear to the shaft, ensuring reliable power transfer in various applications, such as gearboxes, drive systems, and rotary equipment (ARAVIND; ARUL, 2021).

g) Alignment and stability: spline bushes help maintain precise alignment between gears and shafts, ensuring accurate positioning and smooth operation. They resist axial and radial movement, minimizing vibration and reducing the risk of misalignment-related issues (CHEN *et al.*, 2019).

h) Shock and impact resistance: spline bushes are designed to withstand shocks, impacts, and heavy loads encountered in industrial environments. They provide resilience and durability, enhancing the overall robustness of the power

transmission system (HENDERSON *et al.*, 2019).

i) Retrofit and repair: spline bushes are also used for retrofitting or repairing existing power transmission systems. They allow for the replacement of worn or damaged components, extending the lifespan and improving the performance of the machinery (OZEN *et al.*, 2019).

In summary, spline bushes are integral components in power transmission systems. They provide stable and precise connections between gears and shafts, ensuring efficient power transfer, load distribution, and system integrity. Through careful design, material selection, and proper installation, spline bushes contribute to reliable and optimized power transmission in a wide range of applications (MA *et al.*, 2023).

POWER TRANSMISSION CONSIDERATIONS

Power transmission in spur gear systems is influenced by various factors that determine the efficiency, reliability, and overall performance of the system (GRUBKA *et al.*, 2019). This section explores key considerations in power transmission, including gear material, tooth design, lubrication, and the calculation of maximum power capacity.

The choice of gear material significantly impacts the power transmission capabilities of a spur gear system. Factors such as load capacity, operating conditions, and cost considerations play a vital role in material selection (BUDYNAS; NISBETT, 2020). Commonly used gear materials include alloy steels, carbon steels, and non-metallic materials such as plastics or composites (FENG *et al.*, 2020). The selected material must possess high strength, wear resistance, and durability to withstand the forces and contact stresses encountered during operation (NORTON, 2021).

The design of gear teeth is crucial in determining the efficiency and load-carrying capacity of a spur gear system (ALIPIEV, 2011). Factors such as tooth profile, module or pitch, pressure angle, and tooth thickness influence the contact pattern, load distribution, and meshing characteristics (MOTT *et al.*, 2017). Optimal tooth design ensures uniform loading, minimal backlash, and efficient power transmission. CAD software and gear design standards aid in creating accurate tooth profiles that optimize performance (SPECK, 2015).

Proper lubrication is essential for reducing friction, wear, and heat generation in spur gear systems. Lubricants such as oils or greases are applied to the gear teeth to create a lubricating film that minimizes contact and surface damage (ZHAO *et al.*, 2022). Effective lubrication improves gear efficiency by reducing power losses due to friction and heat (LI; KOLIVAND, 2022). Factors such as viscosity, lubricant additives, and lubrication method need to be considered to ensure optimal lubrication and extend the life of the gears (PEI *et al.*, 2021).

Calculating the maximum power capacity of a spur gear system is crucial to ensure reliable and efficient operation. This calculation involves considering various factors such as gear geometry, material properties, tooth profile, and operating conditions. The maximum power capacity determines the upper limit of power that can be safely transmitted without causing excessive wear, overheating, or failure of the gears (DIXIT; KULKARNI, 2023). Properly sizing the gears and verifying their capacity against the expected load helps prevent premature failure and ensures the longevity of the power transmission system (METWALLI, 2021). An example of special reverted planetary gear train is sketched in Figure 6.

ANALYSIS OF INTERFERENCE FIT IN SPLINE BUSHES

Tolerances play a crucial role in the design and implementation of interference fits. An interference fit occurs when two mating components are intentionally designed with dimensions that result in a slight overlap or interference between their surfaces. This interference creates a tight and secure connection between the components. The selection of tolerances is essential to ensure a proper fit between the mating parts. The tolerances must be carefully considered to account for any dimensional variations that may arise during the manufacturing process.

If the tolerances are too tight, it can lead to assembly difficulties or even part damage during the fitting process. On the other hand, if the tolerances are too loose, the interference fit may not be achieved, compromising the desired mechanical integrity and performance of the assembly. Therefore, a thorough understanding of the relationship between tolerances and interference fit is crucial for ensuring the successful implementation of such connections in mechanical systems.

An entry of form tolerances for a spherical pivot with straightness, roundness, and profile form tolerance (surface) and an entry of positional tolerances: hollow bolt with perpendicularity, coaxiality, roundness, and planar runout tolerance are shown in Figure 7.

Interference fit is a critical aspect of the connection between spline bushes and shafts in power transmission systems. This section focuses on the analysis of interference fit in spline bushes, considering the factors that influence its effectiveness and the implications for power transmission (LIU *et al.*, 2023). An example of interference is shown in Figure 8.

Interference fit refers to the intentional interference or tightness between the inner diameter of the spline bush and the outer

diameter of the shaft. This fit creates mechanical interference, ensuring a secure connection and preventing relative motion between the bush and the shaft during operation. The interference fit plays a significant role in maintaining the integrity and performance of the power transmission system (FALHER *et al.*, 2023).

Several factors influence the effectiveness of an interference fit in spline bushes. These include the dimensional tolerances of the bush and shaft, thermal expansion effects, material properties, surface finish, and the amount of interference. The proper consideration and control of these factors are crucial to achieving a reliable interference fit that can withstand the anticipated operational loads and conditions (CARROLL *et al.*, 2023).

Analyzing the interference fit in spline bushes is essential to ensure the reliability and performance of the power transmission system. It helps determine the level of connection strength, resistance to slippage, and the ability to transmit torque without compromising the structural integrity of the components. By analyzing the interference fit, engineers can verify whether the selected dimensions and tolerances are appropriate for the desired power transmission capacity (SUO *et al.*, 2023).

There are various methods available for analyzing the interference fit in spline bushes. These include analytical calculations, finite element analysis (FEA), and experimental testing. Analytical calculations involve considering factors such as the interference amount, the material properties of the bush and shaft, and the contact stresses to estimate the connection strength. FEA allows for more detailed analysis, considering complex geometries, material behavior, and loading conditions (KARALE *et al.*, 2023). Experimental testing involves physically assembling the spline bush and shaft to

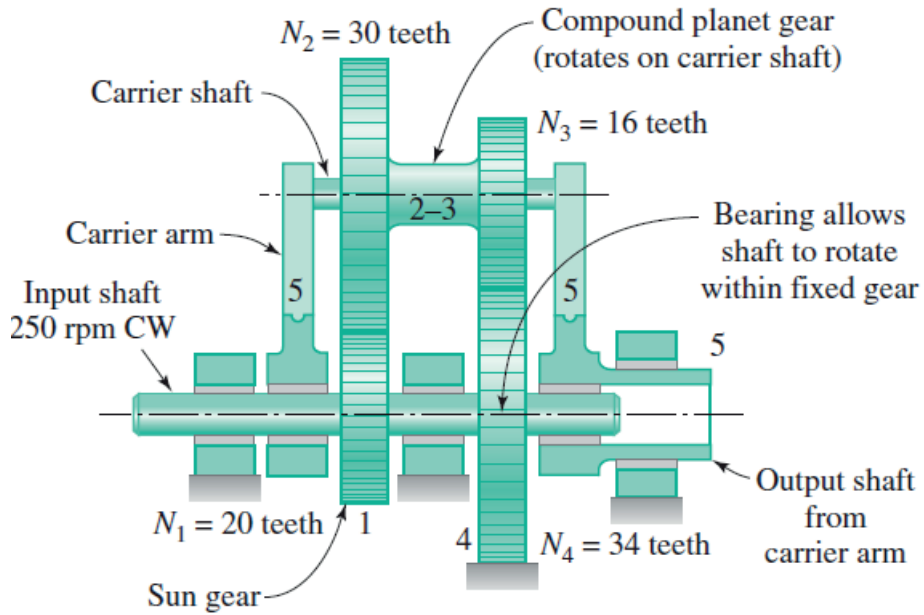


Figure 6 - Reverted compound planetary gear train (COLLINS *et al.*, 2009)

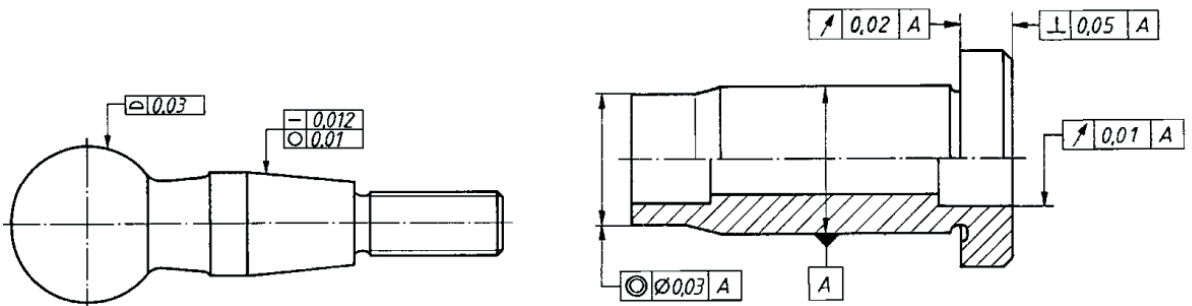


Figure 7 - Form tolerances (left) and Positional tolerances (right) (WITTEL *et al.*, 2011)

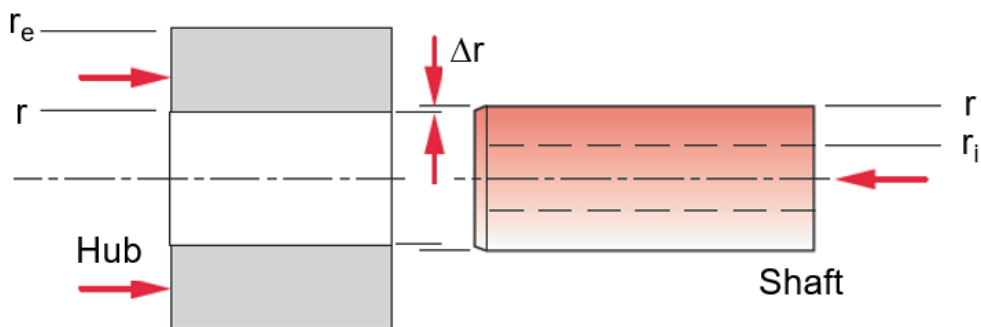


Figure 8 - Interference fit schematics (NORTON, 2021)

measure the level of interference and validate the theoretical predictions (SHU *et al.*, 2022).

The interference fit in spline bushes provides an additional safety feature in power transmission systems. In the event of a torque overload or excessive stress, the interference fit can allow for controlled slippage between the bush and the shaft, preventing mechanical structural failure and potential damage to other system components. This sliding action helps protect the gears, shafts, and other critical elements from catastrophic failure, ensuring the system's overall safety and longevity (ZHOU *et al.*, 2021).

DETERMINING THE MAXIMUM POWER TRANSFER CAPACITY

The maximum power transfer capacity is a critical parameter in the design and operation of power transmission systems. This section focuses on the methods and considerations involved in determining the maximum power transfer capacity of spur gears mounted on shafts with spline bushes and interference fit (LIU *et al.*, 2021). A geared industrial roll is shown in Figure 9.

The maximum power transfer capacity defines the upper limit of power that a gear system can reliably transmit without exceeding its design limits. It ensures that the system can handle the anticipated loads and operating conditions while maintaining performance, efficiency, and longevity. Determining the maximum power transfer capacity is essential for selecting appropriate gear sizes, materials, and operating parameters, thus preventing premature failures and ensuring optimal system performance (LISLE *et al.*, 2017).

Several factors influence the maximum power transfer capacity of spur gears mounted on shafts with spline bushes and interference fit. These factors include gear material properties, tooth design, lubrication, operational speed, temperature,

and the effectiveness of the interference fit. Understanding and accounting for these factors is crucial to accurately determine the system's power transmission limits (HAN *et al.*, 2023).

Various calculation methods can be used to determine the maximum power transfer capacity of a gear system (SÁNCHEZ *et al.*, 2016). These methods involve considering factors such as the gear geometry, tooth strength, contact stresses, surface durability, and material fatigue limits (ČULAR *et al.*, 2022). Standards and empirical formulas developed by organizations such as the American Gear Manufacturers Association (AGMA) provide guidelines and equations for calculating these parameters and estimating the maximum power transfer capacity (CHILDS, 2021). An example of control of transmission error of high contact ratio spur gears with symmetric profile modifications is shown in Figure 10.

Finite Element Analysis (FEA) is a powerful tool for analyzing the behavior of gears and determining their maximum power transfer capacity. FEA enables engineers to model and simulate the complex interactions between gears, spline bushes, shafts, and the interference fit (CHAVADAKI *et al.*, 2021). By applying appropriate material properties, loading conditions, and boundary constraints, FEA can provide detailed insights into stress distribution, deformation, and potential failure modes, helping identify the limiting factors and optimize the system design (AGRAWAL *et al.*, 2022). An example of structural investigation using FEA is shown in Figure 11.

Experimental testing is another valuable approach to determine the maximum power transfer capacity of a gear system. Test setups can be designed to simulate real-world operating conditions and measure parameters such as torque, rotational speed, temperature,

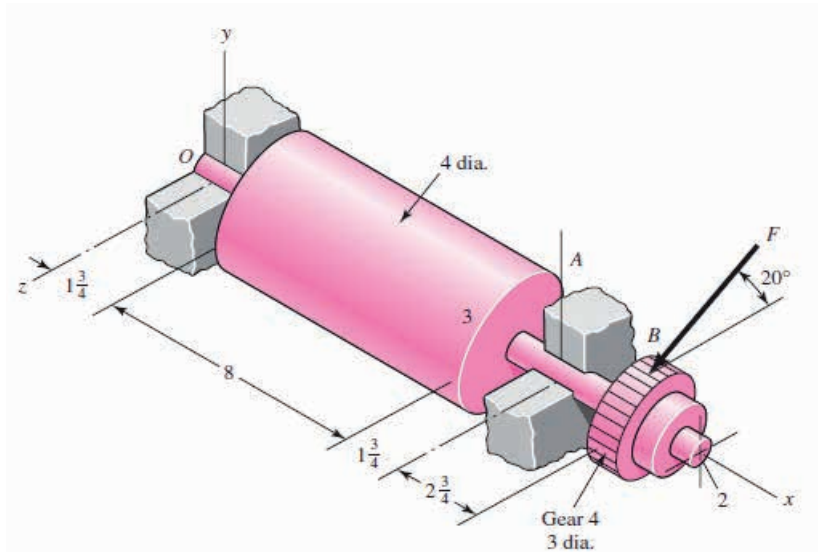


Figure 9 - Geared industrial roll (BUDYNAS; NISBETT, 2020)

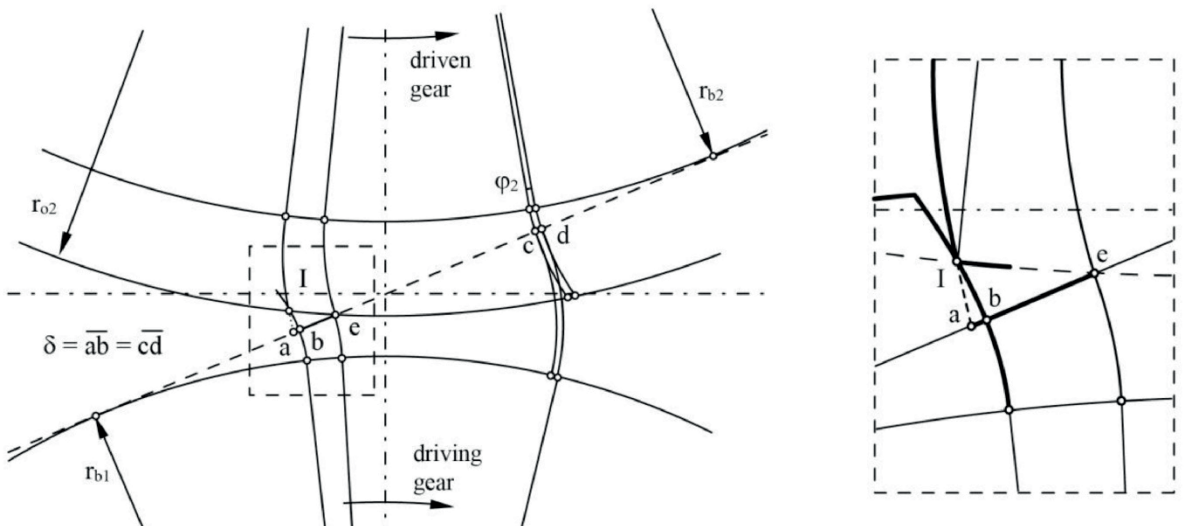


Figure 10 - Load-induced tooth deflections (PLEGUEZUELOS *et al.*, 2020)

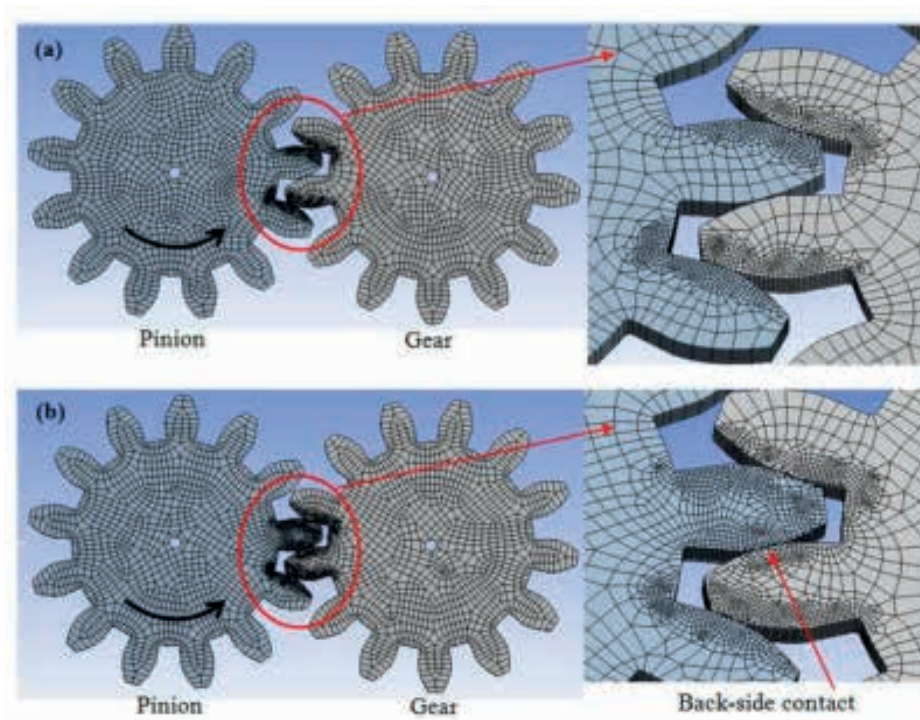


Figure 11 - Finite element models of pinion and gear set (a) without back-side contact (b) with back-side contact (RAGHUWANSHI; PAREY, 2017)

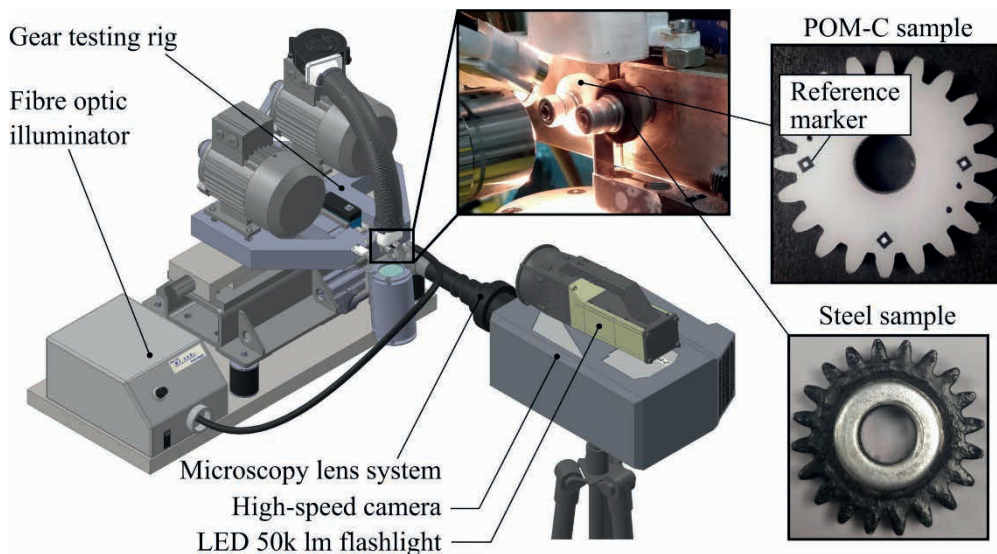


Figure 12 - Presentation of the test equipment setup used in for the experimental analysis (ČERNE; PETKOVĚK, 2022)

and gear performance (GAUDER *et al.*, 2022). By subjecting the gear system to incremental power loads until failure or reaching the desired safety factor, engineers can validate theoretical calculations and gain practical insights into the system's limitations (QIN; GUAN, 2014). An example of high-speed camera-based optical measurement methods for in-mesh tooth deflection analysis of thermoplastic spur gears is shown in Figure 12.

When determining the maximum power transfer capacity, it is crucial to incorporate safety factors and design margins. Safety factors account for uncertainties in operating conditions, material variations, and potential overload situations. Design margins provide an additional buffer to ensure the system's reliability and longevity. The specific safety factors and design margins depend on the industry standards, application requirements, and risk tolerance (ABRUZZO *et al.*, 2023).

CASE STUDY

In this section, we present an example calculation to illustrate the practical application of determining the maximum power transfer capacity for spur gears mounted on shafts with spline bushes and interference fit. This case study provides insights into the calculation process and highlights the considerations involved in determining the power transmission limits.

Consider a power transmission system that utilizes a spur gear mounted on a shaft with a spline bush and an interference fit. A schematic representation of the transmission system with lettered dimensions is shown in Figure 13.

The spur gear is made of cast iron ($E=100$ GPa; $n=0.25$; $\sigma_c=135$ MPa; $\sigma_r=178$ MPa), with a module of 7.25 mm and 25 teeth. The spur gear is attached to an intermediate piece made of carbon steel ($E=203$ GPa; $n=0.29$) with a

strength class of 4.6, using a DIN 5463:1955-09 connection. The intermediate piece undergoes turning externally with an ISO N5 surface finish. However, the internal finishing process of the intermediate piece results in a surface roughness of 10 μm . The dynamic friction coefficient between the intermediate piece and the spur gear is 0.3. The intermediate piece is heat-treated.

The intermediate piece, in turn, is attached to the shaft through an H7t6 fit. The assembly of this intermediate piece on the rotating power transmission shaft occurs through a thermal method. It is known that the shaft is made of bronze ($E=109$ GPa; $n=0.32$; $\sigma_c=56$ MPa; $\sigma_r=67$ MPa) and was milled with a very fine finish. The dynamic friction coefficient between the shaft and the intermediate piece is 0.05.

The system operates at 32°C and is subjected to strong shocks. The torque transmission regime is alternating, and the assembly operates at 300 rpm. Consider that the shaft is subjected to an axial force of 2750 N, and the existing friction between the shaft and the intermediate piece is responsible for supporting this force, along with the transmitted torque.

During the resolution of this statement, we considered the following dimensions in mm: $\varnothing A=40$; $\varnothing C=60$; $T=60$; $N=35$. The dimension $\varnothing B$ was intentionally not provided. Based on this information, it is possible to present the dimensions in Figure 14.

The gear system is subjected to a specific torque load and rotational speed. The goal is to determine the maximum power transfer capacity of the system, considering the gear material, tooth design, lubrication, and efficiency.

Before commencing with the calculations, it is important to outline the resolution strategy to provide readers with a clear understanding of the approach. In Appendix

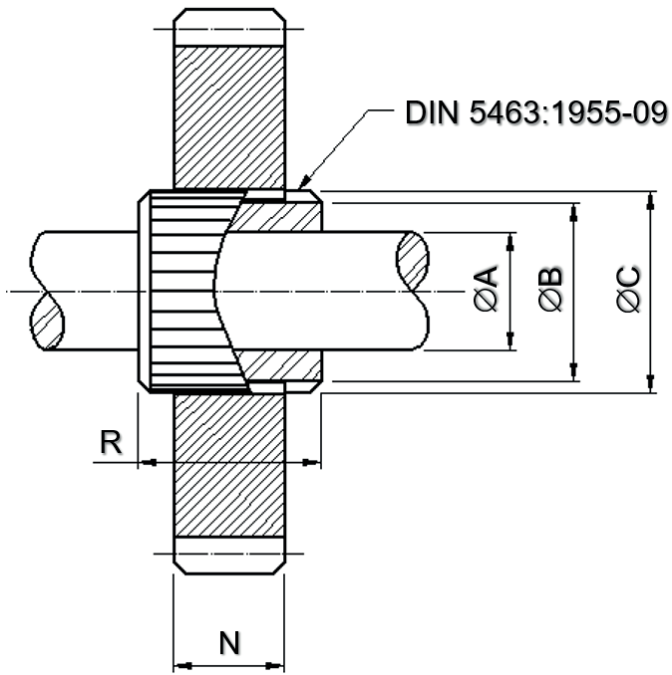


Figure 13 - Schematic representation of the transmission system with lettered dimensions

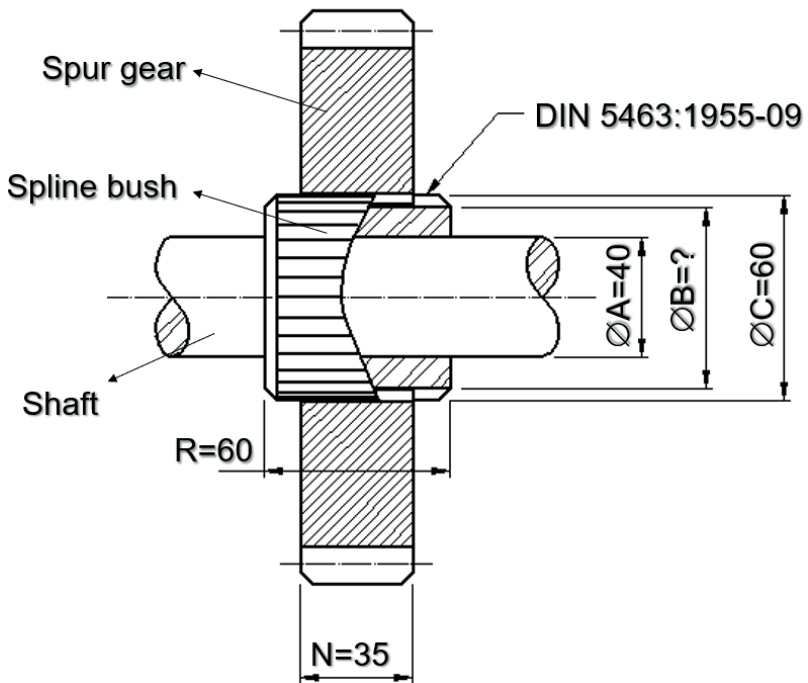


Figure 14 - Schematic representation of the transmission system with current dimensions

A, a compilation of mathematical expressions related to the failure modes of interference fit and spline shafts has been made available. By utilizing these expressions and considering the known material properties and component dimensions, the goal is to determine the maximum torque that the system can transmit.

To achieve this, two different maximum torque values will be calculated. The first value corresponds to the maximum torque allowable to prevent the splined bush from slipping relative to the shaft. Since the bush is mounted using an interference fit, it is crucial to ensure that the applied torque does not exceed this limit, as slippage could compromise the integrity of the transmission system.

The second calculated torque corresponds to the maximum torque allowable to prevent structural damage caused by the failure mode that pertains to the crushing or deformation of components due to excessive contact pressure between the splined bush and the gear hub. It is essential to ensure that the applied torque remains below this limit to avoid any potential structural failures.

After obtaining the two calculated maximum torque values, the lower value between the two will be chosen as the ultimate maximum torque capacity for the system. This approach ensures that both the interference fit integrity and the avoidance of structural damage due to contact pressure are taken into consideration. By selecting the lower value, a conservative and reliable estimation of the system's maximum torque transmission capacity is achieved.

By explaining this resolution strategy, readers will gain a clear understanding of how the calculations will be conducted and the importance of considering both the interference fit and the failure mode related to contact pressure. It highlights the significance of selecting the appropriate torque limit to

ensure the reliability and longevity of the gear system.

To provide readers with a better visualization of the assembly and enhance their understanding of the transmission system, a 3D model has been created. This 3D model can be accessed at the following link: <https://grabcad.com/library/ecdr-montagem-composta-ranhuras-e-interferencia-1>.

The 3D model, offering a comprehensive view of the assembled components, is shown in Figure 15.

To facilitate comprehension, a cross-section of the spur gear is displayed in Figure 16, while the splined bush and shaft are presented without a cross-section. This presentation approach aims to simplify readers' understanding of the system's configuration.

By visually depicting the cross-section of the gear, readers can easily identify the contact area between the spur gear hub and the splined bush, which is established through the use of splines. Additionally, the attachment of the bush to the shaft via interference fit is clearly illustrated.

To facilitate readers' comprehension of the problem's solution, we have included a presentation of important numerical values obtained from literature tables. These values are crucial for performing the calculations and analysis discussed in this article. By providing these values, we aim to assist readers in understanding the practical application of the concepts and methodologies discussed throughout the article.

The statement specifies that the spur gear is made of cast iron, and the power transmission system operates under alternating loads (III) and experiences significant shock loads. The connection between the spur gear and the intermediate piece is achieved through splined shafts. Consequently, it is feasible to determine the permissible pressure (p_{adm}) that

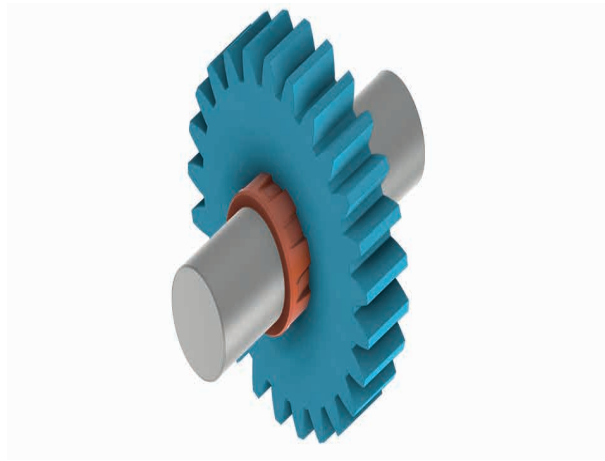


Figure 15 - 3D model of the assembled transmission system

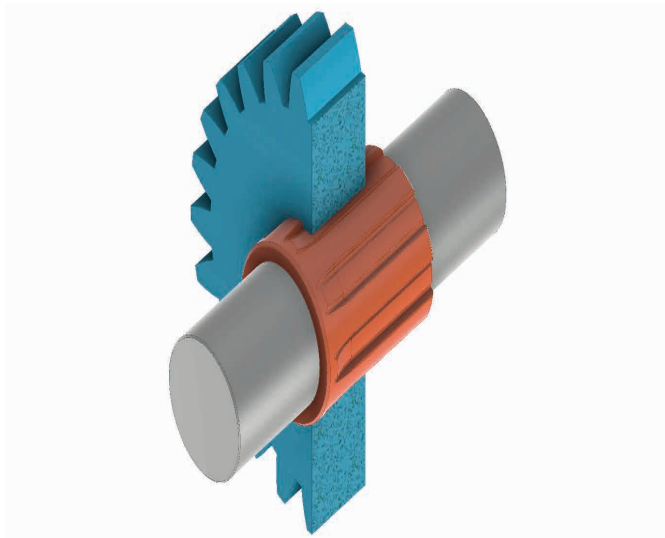


Figure 16 - Schematic representation of the spur gear, splined bush, and shaft assembly

Valores recomendados para p_{adm} [MPa] de uniões de cubos e eixos de aço através de adaptação de forma Fonte: Roloff e Matek (2011)			
Carregamento: choques x tipo de carga	Material do cubo	Chavetas côncavas de aço	Chavetas retangulares de aço, eixos ranhurados de aço
Choques fracos x Carga I ou II	Ferro fundido	40	60
	Aço	65	100
Choques fortes x Carga I ou II	Ferro fundido	25	40
	Aço	50	80
Choques fracos x Carga III	Ferro fundido	20	30
	Aço	33	50
Choques fortes x Carga III	Ferro fundido	13	20
	Aço	25	35

Figure 17 - Determination of the permissible pressure that can be sustained by the interaction between the spur gear and the intermediate piece (adapted and translated from WITTEL *et al.*, 2011)

can be sustained by the interaction between the spur gear and the intermediate piece. The process of obtaining the p_{adm} value is presented in Figure 17.

The statement indicates that the intermediate piece is hardened. Therefore, the value of p_{adm} must be multiplied by 1.5. Therefore, .

It is noted that the statement declares that certain dimensions, in mm, are known. Intentionally, the dimension $\emptyset B$ was omitted to encourage understanding of the technical drawing, as this dimension can be obtained through the dimensional tables of splined shafts, considering that the external diameter of the splined shaft was provided. When interpreting the drawing, it should be understood that the dimension $\emptyset B$ represents the generic dimension d_1 of the splined shafts. On the other hand, the dimension $\emptyset C$ represents the generic dimension d_2 of the splined shafts. Now, as the statement informs that $\emptyset C=60$ mm, it means that we should consult the DIN 5463:1955-09 standard table of splined connections to find the splined shaft that has $d_2=60$ mm. We will then discover that the specification is: $d_1=52$ mm; $d_2=60$ mm; $Z=8$ splines; $b=10$ mm. This identification process in the tables is presented in the following Figure 18.

The arm of the crushing force (r) and the groove height (h) can be calculated respectively, as these are pieces of information that will be used in the application of the crushing failure criterion, which the splined shafts must be verified against.

$$r = \frac{d_2 + d_1}{4} = \frac{60 + 52}{4} = 28 \text{ mm}; h = \frac{d_2 - d_1}{2} = \frac{60 - 52}{2} = 4 \text{ mm}$$

The effective length of contact between the splined shaft and the gear hub (L) corresponds to the dimension $N=35$ mm. Therefore, the criterion for crushing of splined shafts can be

applied to determine the maximum torque that can be transmitted by the splines.

$$\frac{T}{0.75 \cdot Z \cdot r \cdot L \cdot h} \leq p_{adm} \cdot \frac{T}{0.75 \cdot 8 \cdot 28 \cdot 35 \cdot 4} \leq 30 \therefore T \leq 705600 \text{ Nmm}$$

The crushing force acting on the side faces of the splines can be calculated.

$$T = 0.75 \cdot F_{esm} \cdot Z \cdot r \therefore 705600 = 0.75 \cdot F_{esm} \cdot 8 \cdot 28 \therefore F_{esm} = 4200 \text{ N}$$

When analyzing the contact between the rotating shaft and the intermediate component, we must understand that it involves an interference fit. This interference fit occurs between an external component (the intermediate one) and an internal component (the shaft). The contact between these components takes place through the interaction between the internal surface of the intermediate component and the external surface of the rotating shaft. The nominal dimensions of the components are the external diameter of the shaft ($\emptyset A=40$ mm) and the internal diameter of the intermediate component ($\emptyset A= 40$ mm). Therefore, the specification of the fit is 40H7t6. By consulting the fit tables for HOLES and shafts in NBR 6158:1995, we find that: Maximum clearance allowance (A_{max})=25 μm ; Minimum clearance allowance (A_{min}) = 0 μm ; Maximum allowance (a_{max})=64 μm ; Minimum allowance (a_{min})= 48 μm . This process is illustrated in the.

The assembly of these components is performed through thermal expansion. This ensures that there is no loss of interference during the assembly process ($\Delta I=0$).

$$Z_{min} = I_{min} - \Delta I = a_{min} - A_{max} - \Delta I = 48 - 25 - 0 = 23 \mu\text{m}$$

$$Z_{max} = I_{max} - \Delta I = a_{max} - A_{min} - \Delta I = 64 - 0 - 0 = 64 \mu\text{m}$$

The internal component (shaft) and the external component (BORE: intermediate

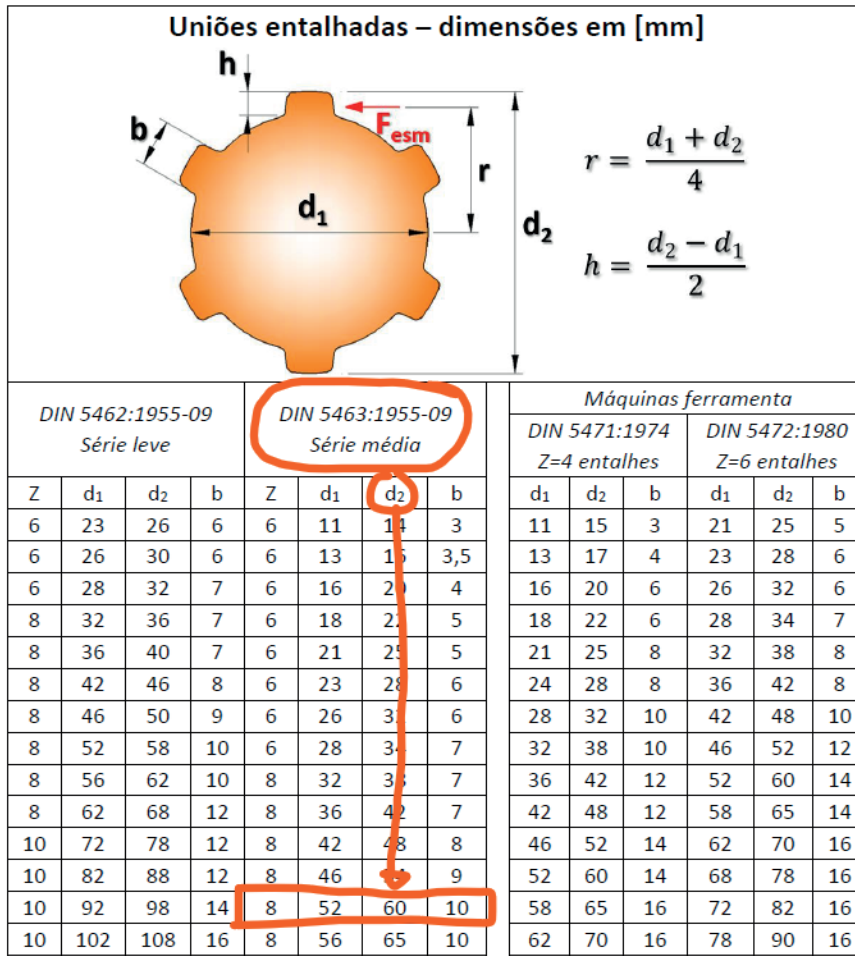


Figure 18 - Splined bush dimensions identification process

dimensão nominal (mm)	IT 5						IT 6						
	p5	r5	s5	t5	u5	v5	x5	p6	r6	s6	u6	v6	x6
até 3	10	14	18	22	24	28	32	12	16	20	24	28	32
mais de 3 a 6	17	20	24	28	33	37	42	20	25	30	35	40	45
mais de 6 a 10	21	25	29	34	40	45	50	24	28	32	37	42	47
mais de 10 a 14	26	31	36	41	48	54	60	28	33	38	44	50	56
mais de 14 a 18	31	37	44	50	58	66	74	33	39	45	52	59	66
mais de 18 a 24	37	44	51	59	68	78	88	39	46	54	62	71	80
mais de 24 a 30	44	52	60	69	79	90	101	46	54	63	73	83	93
mais de 30 a 40	53	62	71	81	92	104	117	54	63	73	84	95	106
mais de 40 a 50	63	73	84	95	107	120	134	63	73	84	95	106	117

Figure 19 - Hub and shaft allowances determination (NBR 6158:1995)

part) need to have their geometric factors determined. The shaft is solid, therefore $Q_i=0$.

$$Q_i = \frac{d_i}{d_e} = \frac{0}{40} = 0$$

On the other hand, the external component is a hollow splined shaft. Hence, the hub has its geometric factor calculated as follows:

$$Q_e = \frac{D_i}{D_e} = \frac{d_1}{d_2} = \frac{40}{52} = 0.769$$

The geometric factors calculations can be illustrated by Figure 20.

As the material properties are provided in the statement, it becomes possible to determine the elastic factors of the components.

$$K_i = \frac{1}{E_i} \cdot \left(\frac{1+Q_i^2}{1-Q_i^2} - \nu_i \right) = \frac{1}{109000} \cdot \left(\frac{1+0^2}{1-0^2} - 0.32 \right) = 6.239 \cdot 10^{-6} \frac{mm^2}{N} = 6.239 \cdot 10^{-6} MPa^{-1}$$

$$K_e = \frac{1}{E_e} \cdot \left(\frac{1+Q_e^2}{1-Q_e^2} + \nu_e \right) = \frac{1}{203000} \cdot \left(\frac{1+0.769^2}{1-0.769^2} + 0.29 \right) = 2.063 \cdot 10^{-6} \frac{mm^2}{N} = 2.063 \cdot 10^{-6} MPa^{-1}$$

The statement indicates that the assembly is radial and will be carried out by cooling the internal component of the joint. It is also known that the system operates at $T_{amb}=32$ °C. Since the internal component of the interference fit is made of bronze, the linear expansion coefficient $a=-15.0 \times 10^{-6}$ oC⁻¹ is determined. This determination process is presented in the Figure 21.

$$T_m = T_{amb} + \frac{I_{max} \cdot 10^{-3} + 5 \cdot 10^{-4} \cdot d}{\alpha \cdot d} = 32 + \frac{64 \cdot 10^{-3} + 5 \cdot 10^{-4} \cdot 40}{-15.0 \cdot 10^{-6} \cdot 40} = -108^\circ C$$

$$\Delta T = T_m - T_{amb} = -108^\circ C - 32^\circ C = -140^\circ C$$

The negative sign indicates that the component should be cooled by 140 °C.

It is possible to calculate the pressure and interference ratios between the HUB and the shaft. From the theory of elasticity, in two-dimensional problems expressed in polar coordinates, the relationship between pressure and interference can be determined.

$$p_{min} = \frac{Z_{min} \cdot 10^{-3}}{(K_i + K_e) \cdot d_{eixo}} = \frac{23 \cdot 10^{-3}}{(6.239 \cdot 10^{-6} + 2.063 \cdot 10^{-6}) \cdot 40} = 21.40 MPa$$

$$p_{max} = \frac{Z_{max} \cdot 10^{-3}}{(K_i + K_e) \cdot d_{eixo}} = \frac{64 \cdot 10^{-3}}{(6.239 \cdot 10^{-6} + 2.063 \cdot 10^{-6}) \cdot 40} = 59.54 MPa$$

The statement states that the dynamic friction coefficient between the shaft and the intermediate piece is 0.05. Therefore, $\mu_D=0.5 \cdot \mu \therefore 0.05=0.5 \cdot \mu \therefore \mu = 0.1$.

The disassembly force can be calculated by $F_d \geq \pi \cdot \mu \cdot k \cdot d \cdot L \cdot p_{max}$. The statement indicates that the safety factor $k=1.8$ and the contact between the rotating shaft and the intermediate piece is $L=60$ mm. Therefore, $F_d = \pi \cdot 0.1 \cdot 1.8 \cdot 40 \cdot 60 \cdot 59.54 = 80808.50N$.

The criterion for no failure to occur is that the acting stress must be less than or equal to the allowable stress. Generally speaking, it can be stated that: $Y \cdot p_{max} \leq \frac{\sigma_e}{n_{mec}}$.

The variable Y refers to the stress concentration factor of each component. As explained during the lectures, this factor is a function of the geometry of each component, depending on the geometric factor of each component. The stress concentration factor of each component should be consulted in the graph provided in the form. Since $Q_i=0$ and $Q_e=0.769$, it is straightforward to determine the stress concentration factors.

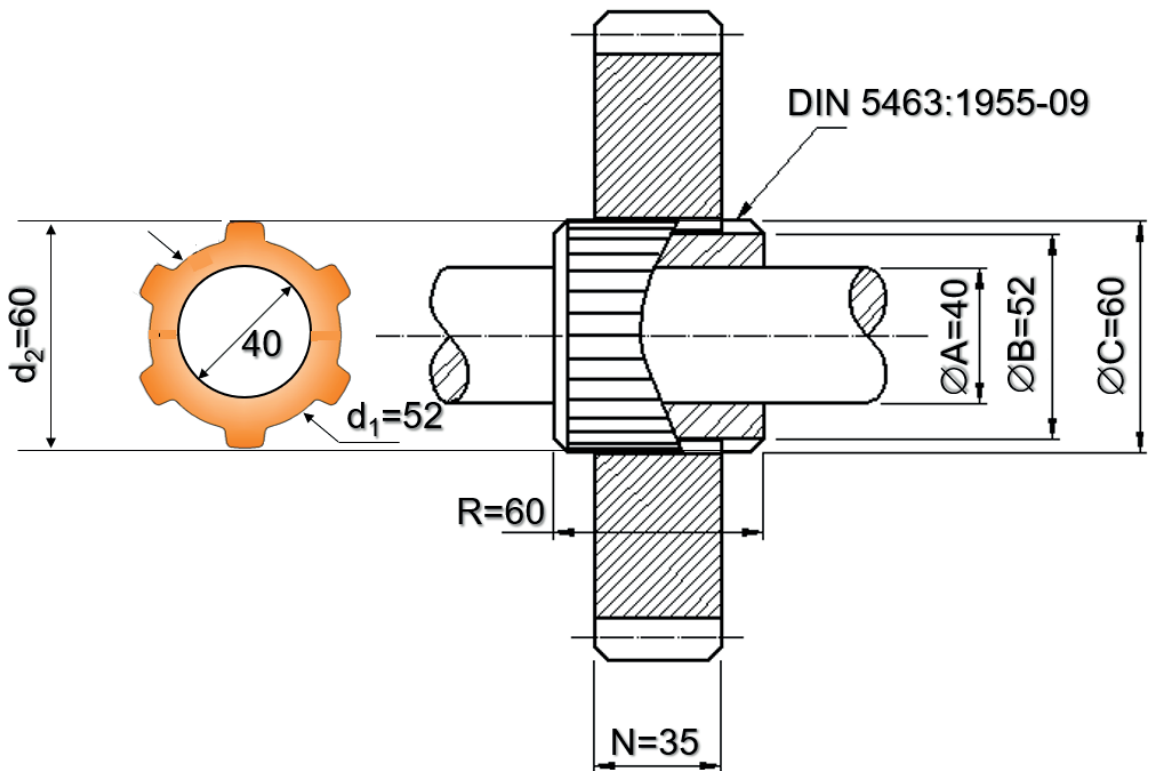
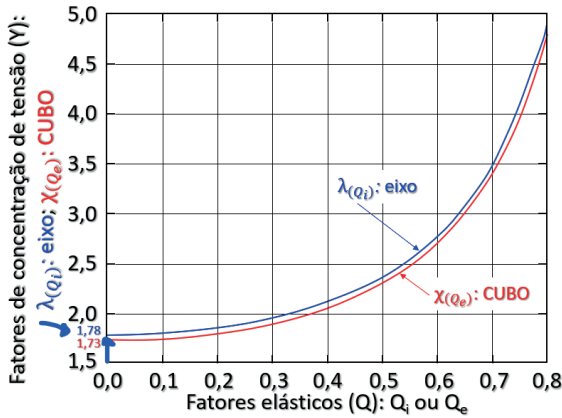


Figure 20 - Geometric factors calculations

Material	E [GPa]	ν	α [°C ⁻¹]	
			Aquecimento	Resfriamento
Aço carbono	203,0	0,29	11,0 × 10 ⁻⁶	-8,5 × 10 ⁻⁶
Aço ligado	207,0	0,29	11,0 × 10 ⁻⁶	-8,5 × 10 ⁻⁶
Ferro fundido dúctil	154,0	0,28	10,0 × 10 ⁻⁶	-8,0 × 10 ⁻⁶
Ferro fundido cinzento	118,0	0,29	10,0 × 10 ⁻⁶	-8,0 × 10 ⁻⁶
Cobre	117,0	0,32	16,0 × 10 ⁻⁶	-14,0 × 10 ⁻⁶
Bronze	109,0	0,32	17,0 × 10 ⁻⁶	-15,0 × 10 ⁻⁶
Latão	104,0	0,32	18,0 × 10 ⁻⁶	-16,0 × 10 ⁻⁶
Alumínio (série 100)	68,4	0,33	24,1 × 10 ⁻⁶	-18,0 × 10 ⁻⁶
Ligas de alumínio	78,4	0,33	23,4 × 10 ⁻⁶	-18,0 × 10 ⁻⁶
Ligas de magnésio	45,3	0,34	26,5 × 10 ⁻⁶	-18,0 × 10 ⁻⁶

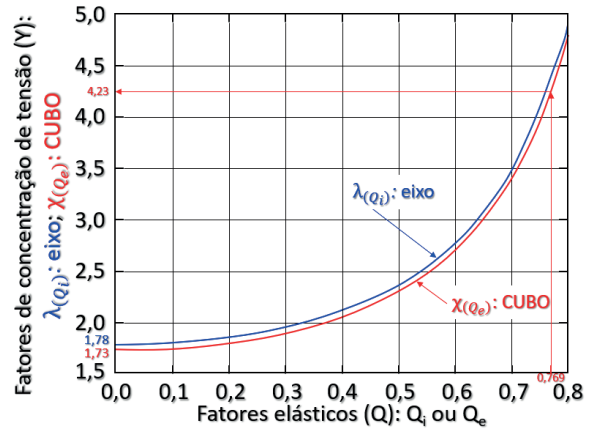
Figure 21 - Linear expansion coefficient determination



$$Y \text{ shaft} \Rightarrow \lambda_{(Q_i=0)} = 1.78$$

$$\text{Shaft: } p_{max} \cdot \lambda_{(Q_i)} \leq \frac{\sigma_{e_{eixo}}}{n_{mec_{eixo}}}$$

$$59.54 \cdot 1.78 \leq \frac{56}{n_{mec_{eixo}}} \therefore n_{mec_{eixo}} = 0.53$$



$$Y \text{ hub} \Rightarrow \chi_{(Q_e=0.769)} = 4.23$$

$$\text{Hub: } p_{max} \cdot \chi_{(Q_e)} \leq \frac{\sigma_{e_{CUBO}}}{n_{mec_{CUBO}}}$$

$$59.54 \cdot 4.23 \leq \frac{240}{n_{mec_{CUBO}}} \therefore n_{mec_{CUBO}} = 0.95$$

This indicates that the component would fail in the event of assembling the larger shaft with the smaller bore (a situation where maximum interference occurs between the components, resulting in maximum pressure between the contact surfaces). It is also noted that the hub would also fail. Therefore, the recommendation would be to make changes to the design. However, it is difficult to provide a specific proposed change or changes as the problem statement did not provide any constraints. Therefore, we suggest considering some of the following measures: improving the mechanical properties of both components, modifying the fit, or altering the geometry of the components in a way that ensures both safety factors are greater than 1. In the case of an exam, exercise, or academic activity, it would be sufficient to provide the calculated numerical values, even if they are less than 1.

The calculation of the transmitted power depends on the relationship between torque

and rotation. This relationship is expressed by the equation: $P = T \cdot \frac{2 \cdot \pi}{60} \cdot n$. In this expression, P represents power [W], T represents torque [Nm], and n represents rotation [rpm]. Since the system's rotation is known, to determine the maximum torque that this joint can safely transmit, we need to calculate the maximum torque that the interference fit can withstand and compare it with the calculated result in item a. Obviously, for safety reasons, we should choose the lower value between these two results. The failure criterion to prevent slippage of the parts joined by interference is:

$$\pi \cdot \mu \cdot d \cdot L \cdot p_{min} \geq \sqrt{F_a^2 + \left(\frac{2 \cdot T}{d}\right)^2} \therefore \pi \cdot 0.1 \cdot 40 \cdot 60 \cdot 21.40 \geq \sqrt{2750^2 + \left(\frac{2 \cdot T}{40}\right)^2}$$

$$T \leq 317950.88 \text{ Nmm}$$

Therefore, the maximum torque is the lower value between the torque transmitted by

the interference fit joint ($T=317,950.88 \text{ Nmm}$) and the splined joint ($T=706,600.00 \text{ Nmm}$). In other words, in this case, the maximum torque is the torque that can be transmitted by the interference fit joint. We just need to calculate the maximum power that can be safely transmitted. It is important to note that in the formula, torque should be used in Nm. So, the equation becomes:

$$P = 317.95 \cdot \frac{2 \cdot \pi}{60} \cdot 300 = 9988.72 \text{ W} = \frac{9988.72}{736} = 13.57 \text{ CV}$$

The results obtained from the calculation example are discussed and interpreted in the context of the specific power transmission system. The calculated maximum power transfer capacity provides valuable insights into the system's capability and aids in the selection of appropriate gear sizes, materials, and operational parameters. The discussion may also include a comparison of the calculated values with industry standards or specific application requirements.

Mechanical applications that utilize spur gears to transmit 13.5 CV include large-scale manufacturing machinery, conveyor systems, machine tools, and automotive drivetrains. The robust nature of spur gears allows them to effectively transmit power while maintaining precise and reliable motion control. Additionally, their design simplicity and compatibility with various shaft configurations make them a preferred choice for high-power applications.

DESIGN CONSIDERATIONS AND OPTIMIZATION TECHNIQUES

Designing a robust and efficient power transmission system involves careful consideration of various factors and the application of optimization techniques (APPARAO; RAJU, 2021). This section

explores the key design considerations and optimization techniques that can enhance the performance, reliability, and longevity of spur gears mounted on shafts with spline bushes and interference fit.

The tooth profile and geometry of the spur gears have a significant impact on their performance. Design considerations such as the pressure angle, module or pitch, tooth thickness, and addendum modification factor influence factors like load distribution, contact stresses, and noise generation. Optimizing the tooth profile and geometry ensures efficient power transmission, reduced noise, and improved durability (CHI *et al.*, 2022).

Choosing the appropriate gear material and applying suitable heat treatment processes is crucial for achieving the desired mechanical properties and performance characteristics. Factors such as strength, wear resistance, and fatigue resistance should be considered. Material selection should also account for factors such as cost, availability, and environmental considerations. Heat treatment processes such as carburizing, quenching, and tempering can further enhance the material properties and improve gear performance (ASLANTAŞ *et al.*, 2004).

Proper lubrication and surface coatings play a vital role in reducing friction, wear, and heat generation in power transmission systems. Selecting the right lubricant based on factors like viscosity, additives, and operating conditions ensures optimal lubrication. Surface coatings such as hardening treatments, coatings, or platings can improve wear resistance and reduce friction, enhancing the overall efficiency and durability of the gears (KARTHICK *et al.*, 2023).

Noise and vibration are common concerns in power transmission systems. Design considerations such as gear tooth profile optimization, proper backlash control, and the use of damping techniques can help

mitigate noise and vibration issues (NING *et al.*, 2021). By minimizing the excitation forces and optimizing gear geometry, noise and vibration levels can be significantly reduced, improving the overall performance and user experience (SINGH *et al.*, 2022).

Optimization techniques such as computer-aided design (CAD), computer-aided engineering (CAE), and numerical optimization methods can greatly aid in the design and optimization of power transmission systems (GAO *et al.*, 2022). CAD software enables engineers to create accurate 3D models, analyze gear performance, and simulate operating conditions (KISHORE *et al.*, 2022). CAE tools, such as finite element analysis (FEA), can provide insights into stress distribution, deformation, and potential failure modes, aiding in design optimization (KURBET *et al.*, 2022). Numerical optimization methods can be employed to iteratively optimize design parameters and maximize system performance (KULANGARA *et al.*, 2018).

Reliability assessment and failure analysis are essential for ensuring the longevity and safe operation of power transmission systems (NAMBOOTHIRI *et al.*, 2022). Failure modes, such as tooth breakage, wear, or pitting, should be analyzed to identify the root causes and implement design improvements (KADER *et al.*, 1998). Techniques like failure mode and effects analysis (FMEA) can help identify potential failure modes and develop mitigation strategies to enhance system reliability (CAMERON *et al.*, 2023).

CONCLUSIONS

In this technical article, we have explored the determination of the maximum power transfer capacity of spur gears mounted on shafts with spline bushes using an interference fit. Through a comprehensive analysis of spur gears, spline bushes, and the benefits of

an interference fit, we have gained valuable insights into the design and optimization of gear systems.

By accurately calculating the maximum power capacity, engineers can make informed decisions in gear system design to ensure reliable and efficient operation. The use of an interference fit in spline bushes not only provides enhanced stability and load distribution but also introduces a safety mechanism. In the event of torque overload or sudden shock load, the interference fit allows the spline bush to slip on the shaft, preventing mechanical structural failure and safeguarding the transmission elements.

We have discussed critical factors that influence power transmission, including tooth strength, contact stress, and bending fatigue. Analytical methods and calculations have been presented, enabling engineers to determine these parameters accurately. The case study showcased the application of these methods in practical scenarios, illustrating their effectiveness in determining the maximum power transfer capacity.

Design considerations and optimization techniques have been explored to enhance power capacity. These include tooth profile modification, material selection, and improvements in lubrication. By leveraging these strategies and iteratively refining gear system designs, engineers can maximize performance while ensuring long-term reliability and safety.

In conclusion, determining the maximum power transfer capacity of spur gears mounted on shafts with spline bushes using an interference fit is crucial for designing robust and efficient gear systems. The insights and methodologies presented in this article provide valuable guidance for engineers in achieving optimal power transmission, considering safety aspects, and meeting the demands of various industrial applications.

As future advancements continue to shape the field of gear system design, further research may focus on exploring advanced materials, optimizing tooth profiles, and refining analytical techniques. By staying at the forefront of innovation, engineers can continue to push the boundaries of power transmission and develop even more reliable and efficient gear systems.

ACKNOWLEDGEMENTS

The authors would like to express their sincere gratitude to their families for their unwavering support throughout the course of this research. We would also like to acknowledge the academics institutions Fatec Diadema and Centro Universitário FEI for providing us with the necessary resources and infrastructure to carry out this work.

REFERENCES

- [1] ABNT. NBR 6158. **Sistema de tolerâncias e ajustes**. 1995.
- [2] ABRUZZO, M.; BEGHINI, M.; SANTUS, C.; PRESICCE, F. A dynamic model combining the average and the local meshing stiffnesses and based on the static transmission error for spur gears with profile modification. **Mechanism And Machine Theory**, [S.L.], v. 180, p. 105139, Feb. 2023. Elsevier BV. <http://dx.doi.org/10.1016/j.mechmachtheory.2022.105139>.
- [3] AGRAWAL, Anant Prakash; ALI, Shahazad; RATHORE, Sachin. Finite element stress analysis for shape optimization of spur gear using ANSYS. **Materials Today: Proceedings**, [S.L.], v. 64, p. 1147-1152, 2022. Elsevier BV. <http://dx.doi.org/10.1016/j.matpr.2022.03.404>.
- [4] ALIPIEV, Ognyan. Geometric design of involute spur gear drives with symmetric and asymmetric teeth using the Realized Potential Method. **Mechanism And Machine Theory**, [S.L.], v. 46, n. 1, p. 10-32, Jan. 2011. Elsevier BV. <http://dx.doi.org/10.1016/j.mechmachtheory.2010.09.001>.
- [5] APPARAO, D.; RAJU, M.V. Jagannadha. Design and analysis of spur gear manufactured by DMLS process. **Materials Today: Proceedings**, [S.L.], v. 46, p. 149-153, 2021. Elsevier BV. <http://dx.doi.org/10.1016/j.matpr.2020.07.078>.
- [6] ARAVIND, T.V.; ARUL, Sanjivi. Effect of deep cryogenic treatment on C93700 bearing bush material used in submersible pumps. **Materials Today: Proceedings**, [S.L.], v. 46, p. 4685-4690, 2021. Elsevier BV. <http://dx.doi.org/10.1016/j.matpr.2020.10.297>.
- [7] ASLANTAŞ, K.; TAŞGETIREN, S.; YALÇINDAN, Y.. Austempering retards pitting failure in ductile iron spur gears. **Engineering Failure Analysis**, [S.L.], v. 11, n. 6, p. 935-941, Dec. 2004. Elsevier BV. <http://dx.doi.org/10.1016/j.engfailanal.2003.12.002>.
- [8] BAUMANN, Andreas; MAY, David; HAUSMANN, Joachim. Characterization of metallic bushings in RTM-made composites by in-situ leak detection under mechanical loading. **Composites Part C: Open Access**, [S.L.], v. 7, p. 100226, Mar. 2022. Elsevier BV. <http://dx.doi.org/10.1016/j.jcomc.2021.100226>.
- [9] BHANDARI, V. B.. **Design of Machine Elements**. 3. ed. McGraw-Hill, 2010. 958 p. (ISBN-13: 978-0070681798).
- [10] BUDYNAS, Richard; NISBETT, Keith. **Shigley's Mechanical Engineering Design**. 11. ed. McGraw-Hill, 2020. (ISBN10: 0073398217). <https://www.mheducation.com/highered/product/shigley-s-mechanical-engineering-design-budynas-nisbett/M9780073398211.html>.
- [11] CAMERON, Zachary A.; KRANTZ, Timothy L.. Statistical distribution of gear surface fatigue lives at high reliability. **International Journal Of Fatigue**, [S.L.], v. 167, p. 107350, Feb. 2023. Elsevier BV. <http://dx.doi.org/10.1016/j.ijfatigue.2022.107350>.
- [12] CARROLL, Jordan; KHATIBI, Akbar A.; ROBERTSON, Leigh; BARTER, Simon. Observations of non-linear stress effects on crack growth in interference fit fasteners. **International Journal Of Fatigue**, [S.L.], v. 167, p. 107319, Feb. 2023. Elsevier BV. <http://dx.doi.org/10.1016/j.ijfatigue.2022.107319>.
- [13] ČERNE, B.; PETKOVĚK, M.. High-speed camera-based optical measurement methods for in-mesh tooth deflection analysis of thermoplastic spur gears. **Materials & Design**, [S.L.], v. 223, p. 111184, Nov. 2022. Elsevier BV. <http://dx.doi.org/10.1016/j.matdes.2022.111184>.

- [14] CHANG, Xuefeng; RENQING, Duoji; LIAO, Longxing; ZHU, Peiyuan; LIN, Bingjing; HUANG, Yubin; LUO, Shanming. Study on hydrodynamic lubrication and friction reduction performance of spur gear with groove texture. **Tribology International**, [S.L.], v. 177, p. 107978, Jan. 2023. Elsevier BV. <http://dx.doi.org/10.1016/j.triboint.2022.107978>.
- [15] CHAVADAKI, Subhash; KUMAR, K.C. Nithin; RAJESH, M.N.. Finite element analysis of spur gear to find out the optimum root radius. **Materials Today: Proceedings**, [S.L.], v. 46, p. 10672-10675, 2021. Elsevier BV. <http://dx.doi.org/10.1016/j.matpr.2021.01.422>.
- [16] CHEN, Jie; YANG, Zhen-Guo. Cause analysis on the unqualified pull-out force between the bushing and PCB pad in DC-DC converters for new energy vehicles. **Engineering Failure Analysis**, [S.L.], v. 145, p. 107012, Mar. 2023. Elsevier BV. <http://dx.doi.org/10.1016/j.engfailanal.2022.107012>.
- [17] CHEN, Shi; YIN, Nian; YU, Qin; ZHANG, Zhinan. A novel tribometer for investigating bushing wear. **Wear**, [S.L.], v. 430-431, p. 263-271, Jul. 2019. Elsevier BV. <http://dx.doi.org/10.1016/j.wear.2019.05.014>.
- [18] CHI, Yifei; ZHAO, Yaping; ZHU, Xinyue; LI, Gongfa; CHEN, Xinyuan. Mismatched gearing composed of hourglass worm and spur gear: meshing theory, tooth contact simulation, comprehensive design. **Mechanism And Machine Theory**, [S.L.], v. 174, p. 104883, Aug. 2022. Elsevier BV. <http://dx.doi.org/10.1016/j.mechmachtheory.2022.104883>.
- [19] CHILDS, P.R.N.. Spur and Helical Gear Stressing. **Mechanical Design**, [S.L.], p. 209-236, 2021. Elsevier. <http://dx.doi.org/10.1016/b978-0-12-821102-1.00006-8>.
- [20] COLLINS, Jack A.; BUSBY, Henry R.; STAAB, George H.. **Mechanical Design of Machine Elements and Machines: failure prevention perspective**. 2. ed. Wiley, 2009. 912 p. (ISBN: 978-0-470-41303-6). <https://www.wiley.com/en-us/Mechanical+Design+of+Machine+Elements+and+Machines%3A+A+Failure+Prevention+Perspective%2C+2nd+Edition-p-9780470413036>.
- [21] ČULAR, Ivan; VUČKOVIĆ, Krešimir; GLODEŽ, Srečko; TONKOVIĆ, Zdenko. Computational model for bending fatigue prediction of surface hardened spur gears based on the multilayer method. **International Journal Of Fatigue**, [S.L.], v. 161, p. 106892, Aug. 2022. Elsevier BV. <http://dx.doi.org/10.1016/j.ijfatigue.2022.106892>.
- [22] CUI, Wenyan; XU, Mingkun; TAO, Liming; WANG, Tingmei; YU, Chengguo; LIANG, Bo; MA, Tianbao. In-situ observation of transfer film formation and evolution for the fabric composite lubricated spherical plain bearing at cryogenic and wide temperature range. **Applied Surface Science**, [S.L.], v. 612, p. 155946, Mar. 2023. Elsevier BV. <http://dx.doi.org/10.1016/j.apsusc.2022.155946>.
- [23] DING, Han; LI, Hongping; CHEN, Siyu; SHI, Yingjie; WANG, Yongsheng; RONG, Kaibin; LU, Rui. Energy loss and mechanical efficiency forecasting model for aero-engine bevel gear power transmission. **International Journal Of Mechanical Sciences**, [S.L.], v. 231, p. 107569, Oct. 2022. Elsevier BV. <http://dx.doi.org/10.1016/j.ijmecsci.2022.107569>.
- [24] DIXIT, Yashanshu; KULKARNI, Makarand S.. Multi-objective optimization with solution ranking for design of spur gear pair considering multiple failure modes. **Tribology International**, [S.L.], v. 180, p. 108284, Feb. 2023. Elsevier BV. <http://dx.doi.org/10.1016/j.triboint.2023.108284>.
- [25] DUDEK, K.K.; MIZZI, L.; MARTÍNEZ, J.A. Iglesias; SPAGGIARI, A.; ULLIAC, G.; GATT, R.; GRIMA, J.N.; LAUDE, V.; KADIC, M.. Micro-scale graded mechanical metamaterials exhibiting versatile poisson's ratio. **Composite Structures**, [S.L.], p. 117151, May 2023. Elsevier BV. <http://dx.doi.org/10.1016/j.compstruct.2023.117151>.
- [26] DUNCHEVA, G.V.; MAXIMOV, J.T.; ANCHEV, A.P.; DUNCHEV, V.P.; ARGIROV, Y.B.; KANDEVA-IVANOVA, M.. Enhancement of the wear resistance of CuAl9Fe4 sliding bearing bushings via diamond burnishing. **Wear**, [S.L.], v. 510-511, p. 204491, Dec. 2022. Elsevier BV. <http://dx.doi.org/10.1016/j.wear.2022.204491>.
- [27] FALHER, M. Le; FOUVRY, S.; ARNAUD, P.; MAUREL, V.; ANTONI, N.; BILLARDON, R.. FRETTING-FATIGUE OF SHRINK FIT LUG-BUSH ASSEMBLIES: interference-fit effect. **Tribology International**, [S.L.], p. 108581, May 2023. Elsevier BV. <http://dx.doi.org/10.1016/j.triboint.2023.108581>.
- [28] FENG, Wei; JIA, Xiangyang; LIU, Biao; GAO, Ming. Material flow characteristics and deformation law during dual directional hot forging of the steel-aluminium spur gear. **Procedia Manufacturing**, [S.L.], v. 50, p. 425-428, 2020. Elsevier BV. <http://dx.doi.org/10.1016/j.promfg.2020.08.077>.

- [29] GAUDER, Daniel; GÖLZ, Johannes; HORNING, Nils; LANZA, Gisela. Uncertainty determination of a novel single flank rolling test facility for micro spur gears. **Cirp Journal Of Manufacturing Science And Technology**, [S.L.], v. 39, p. 332-344, Nov. 2022. Elsevier BV. <http://dx.doi.org/10.1016/j.cirpj.2022.08.014>.
- [30] GAO, Pu; LIU, Hui; YAN, Pengfei; XIE, Yunkun; XIANG, Changle; WANG, Cheng. Research on application of dynamic optimization modification for an involute spur gear in a fixed-shaft gear transmission system. **Mechanical Systems And Signal Processing**, [S.L.], v. 181, p. 109530, Dec. 2022. Elsevier BV. <http://dx.doi.org/10.1016/j.ymsp.2022.109530>.
- [31] GRAZIOSO, Stanislao; GIRONIMO, Giuseppe di; SICILIANO, Bruno. Modeling and vibration control of flexible mechanical systems for DEMO remote maintenance: results from the flexarm project. **Fusion Engineering And Design**, [S.L.], v. 146, p. 1423-1425, Sep. 2019. Elsevier BV. <http://dx.doi.org/10.1016/j.fusengdes.2019.02.096>.
- [32] GRUBKA, R.M.; PICHKO, N.s.; PETRYAYEVA, I.A.; MIKHAILOV, A.N.. Some features of the design and technological preparation of the production of spur gears with spatially modified teeth. **Materials Today: Proceedings**, [S.L.], v. 19, p. 2483-2487, 2019. Elsevier BV. <http://dx.doi.org/10.1016/j.matpr.2019.08.163>.
- [33] GUPTA, Kapil; JAIN, Neelesh Kumar. Analysis and optimization of micro-geometry of miniature spur gears manufactured by wire electric discharge machining. **Precision Engineering**, [S.L.], v. 38, n. 4, p. 728-737, Oct. 2014. Elsevier BV. <http://dx.doi.org/10.1016/j.precisioneng.2014.03.009>.
- [34] HAN, Xinghui *et al.* Transmission performance evaluation of non-circular spur bevel gear based on a novel isochronal measurement method. **Mechanism And Machine Theory**, [S.L.], v. 185, p. 105329, Jul. 2023. Elsevier BV. <http://dx.doi.org/10.1016/j.mechmachtheory.2023.105329>.
- [35] HENDERSON, Christine N.; DEFRANCE, Charles S.; PREDECKI, Paul; KUMOSA, Maciej. Damage prevention in transformer bushings subjected to high-velocity impact. **International Journal Of Impact Engineering**, [S.L.], v. 130, p. 1-10, Aug. 2019. Elsevier BV. <http://dx.doi.org/10.1016/j.ijimpeng.2019.03.007>.
- [36] HUSSEIN, Ahmed W.; ABDULLAH, Mohammad Q. High-contact ratio spur gears with conformal contact and reduced sliding. **Results In Engineering**, [S.L.], v. 14, p. 100412, jun. 2022. Elsevier BV. <http://dx.doi.org/10.1016/j.rineng.2022.100412>.
- [37] ISLAM, Md Din; NURUNNABI, Md; MRIDULA, Fairouz Raisa; MIA, Rony; BELAL, Shah Alimuzzaman. A cost-effective approach after implementation of timing belt drive in the cotton ring-spinning frame. **Cleaner Engineering And Technology**, [S.L.], v. 9, p. 100536, Aug. 2022. Elsevier BV. <http://dx.doi.org/10.1016/j.clet.2022.100536>.
- [38] JADON, V K.; VERMA, Suresh. **Analysis and Design of Machine Elements**. 2. ed. New Delhi - 110002, Delhi, India: I.K International Pvt. Ltd., 2014. 1000 p. (ISBN: 9789384588106). <https://www.ikbooks.com/books/book/engineering-computer-science/mechanical-production-industrial-engineering/analysis-design-machine-elements/9789384588106/>
- [39] JIANG, Wei. **Analysis and Design of Machine Elements**. Wiley, 2019. 528 p. (ISBN: 978-1-119-27607-4). <https://www.wiley.com/en-us/Analysis+and+Design+of+Machine+Elements-p-9781119276074>
- [40] JIANG, Deyin; CHEN, Tianyu; XIE, Juanzhang; CUI, Weimin; SONG, Bifeng. A mechanical system reliability degradation analysis and remaining life estimation method—With the example of an aircraft hatch lock mechanism. **Reliability Engineering & System Safety**, [S.L.], v. 230, p. 108922, Feb. 2023a. Elsevier BV. <http://dx.doi.org/10.1016/j.res.2022.108922>.
- [41] JIANG, Fei; DING, Kang; ZHANG, Shaohui; WU, Zhaoqian; HE, Guolin. Vibration response mechanism of fixed-shaft gear train with cracks based on rigid-flexible coupling dynamics and signal convolution model. **Mechanical Systems And Signal Processing**, [S.L.], v. 198, p. 110417, Sep. 2023b. Elsevier BV. <http://dx.doi.org/10.1016/j.ymsp.2023.110417>.
- [42] JUVINALL, Robert C.; MARSHEK, Kurt M.. **Fundamentals of Machine Component Design**. 7. ed: Wiley, 2019. 800 p. (ISBN: 978-1-119-47568-2). <https://www.wiley.com/en-br/Fundamentals+of+Machine+Component+Design%2C+7th+Edition-p-9781119475682>.
- [43] KADER, Mushtaq M.A.; NIGAM, S.P.; GROVER, G.K.. A study on mode of failures in spur gears under optimized conditions. **Mechanism And Machine Theory**, [S.L.], v. 33, n. 6, p. 839-850, Aug. 1998. Elsevier BV. [http://dx.doi.org/10.1016/S0094-114X\(97\)00058-X](http://dx.doi.org/10.1016/S0094-114X(97)00058-X).

- [44] KARALE, Ajinkya; MOHANKUMAR, V.; RANE, Sandeep. Evaluate slip torque of an interference fit using preloaded, non-linear large strain simulation in MSC MARC. **Materials Today: Proceedings**, [S.L.], v. 72, p. 1890-1895, 2023. Elsevier BV. <http://dx.doi.org/10.1016/j.matpr.2022.10.151>.
- [45] KARTHICK, M.; RAMAKRISHNA, Ch. Siva; PUGAZHENTHI, R.; GUDADHE, Nitin; BASKAR, S.; RENU; KUMAR, Rajan. Contact stress analysis of xylon coated spur gear using ANSYS workbench. **Materials Today: Proceedings**, [S.L.], v. 5, n. 8, p. 327-345, Apr. 2023. Elsevier BV. <http://dx.doi.org/10.1016/j.matpr.2023.03.572>.
- [46] KISHORE, Samala Nanda; REDDY, Alla Vishnu Vardhan; RAO, Lokavarapu Bhaskara. Design and optimization of spur gears in a single stage reduction gear box. **Materials Today: Proceedings**, [S.L.], v. 60, p. 2010-2017, 2022. Elsevier BV. <http://dx.doi.org/10.1016/j.matpr.2022.01.258>.
- [47] KULANGARA, Arun J.; RAO, C.s.P.; BOSE, P. Subhash Chandra. Generation and optimization of lattice structure on a spur gear. **Materials Today: Proceedings**, [S.L.], v. 5, n. 2, p. 5068-5073, 2018. Elsevier BV. <http://dx.doi.org/10.1016/j.matpr.2017.12.085>.
- [48] KUMAR, Rahul; KUMAR, Dharmendra; MAHATO, Anil C.; TRIPATHI, Jay P.. Dynamic modeling and analysis of a hydro-mechanical power transmission system. **Materials Today: Proceedings**, [S.L.], v. 61, p. 50-54, 2022. Elsevier BV. <http://dx.doi.org/10.1016/j.matpr.2022.03.311>.
- [49] KURBET, Ramesh; DODDASWAMY, V.; AMRUTH, C.M.; KERUR, Mohammedrafi H.; GHANARAJA, S.. Frequency response analysis of spur gear pair using FEA. **Materials Today: Proceedings**, [S.L.], v. 52, p. 2327-2338, 2022. Elsevier BV. <http://dx.doi.org/10.1016/j.matpr.2021.12.517>.
- [50] LI, S.; KOLIVAND, A.. Crack nucleation and propagation modeling for lubricated spur gear contacts of rough surfaces. **Mechanism And Machine Theory**, [S.L.], v. 170, p. 104726, Apr. 2022. Elsevier BV. <http://dx.doi.org/10.1016/j.mechmachtheory.2022.104726>.
- [51] LISLE, Timothy J.; SHAW, Brian A.; FRAZER, Robert C.. External spur gear root bending stress: a comparison of iso 6336. **Mechanism And Machine Theory**, [S.L.], v. 111, p. 1-9, May 2017. Elsevier BV. <http://dx.doi.org/10.1016/j.mechmachtheory.2017.01.006>.
- [52] LIU, Pengfei; ZHU, Lingyun; GOU, Xiangfeng; SHI, Jianfei; JIN, Guoguang. Modeling and analyzing of nonlinear dynamics for spur gear pair with pitch deviation under multi-state meshing. **Mechanism And Machine Theory**, [S.L.], v. 163, p. 104378, Sep. 2021. Elsevier BV. <http://dx.doi.org/10.1016/j.mechmachtheory.2021.104378>.
- [53] LIU, Siyuan; CHEN, Xiaojin; SONG, Chaosheng; ZHU, Caichao; BAI, Houyi; FUENTES-AZNAR, Alfonso. Influence of gear-shaft interference fit assembly on the meshing characteristics of cylindrical gears considering comprehensive modifications. **Mechanism And Machine Theory**, [S.L.], v. 182, p. 105247, Apr. 2023. Elsevier BV. <http://dx.doi.org/10.1016/j.mechmachtheory.2023.105247>.
- [54] MA, Xinxing; SONG, Yuxiang; CAO, Peng; LI, Jian; ZHANG, Zhenguo. Self-excited vibration suppression of a spline-shafting system using a nonlinear energy sink. **International Journal Of Mechanical Sciences**, [S.L.], v. 245, p. 108105, May 2023. Elsevier BV. <http://dx.doi.org/10.1016/j.ijmecsci.2023.108105>.
- [55] MELCONIAN, Sarkis. **Elementos de Máquinas**. 11. ed. Érica, 2019. 384 p. (ISBN 9788536530437). <https://www.editoraerica.com.br/elementos-de-maquinas---11%C2%AA-edicao/p>.
- [56] METWALLI, Sayed M.. **Machine Design with CAD and Optimization**. Wiley, 2021. 1008 p. (ISBN: 978-1-119-15664-2). <https://www.wiley.com/en-us/Machine+Design+with+CAD+and+Optimization-p-9781119156642>.
- [57] MOTT, Robert L.; VAVREK, Edward M.; WANG, Jyhwen. **Machine Elements in Mechanical Design**. 6. ed. Pearson, 2017. (ISBN-13: 9780134441184). <https://www.pearson.com/en-us/subject-catalog/p/machine-elements-in-mechanical-design/P200000001541/9780134441184>.
- [58] MU, Shibo; ZHAO, Yaping; CUI, Jian; MENG, Qingxiang; LI, Gongfa. Meshing theory of face worm gear drive with hardened cylindrical worm. **Mechanism And Machine Theory**, [S.L.], v. 185, p. 105323, Jul. 2023. Elsevier BV. <http://dx.doi.org/10.1016/j.mechmachtheory.2023.105323>.

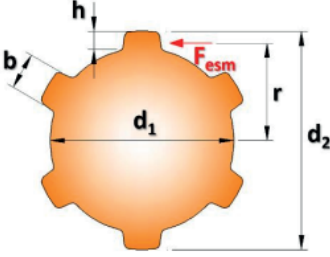
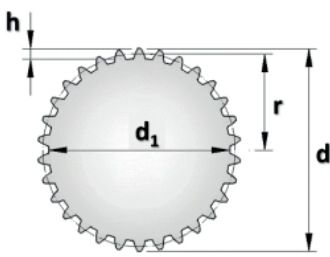
- [59] NAMBOOTHIRI, Nandu V.; MARIMUTHU, P.; KUMAR, S. Suresh. Analysis of fracture characteristics of thin and thick rim asymmetric spur gear based on strain energy release rate. **Theoretical And Applied Fracture Mechanics**, [S.L.], v. 121, p. 103496, Oct. 2022. Elsevier BV. <http://dx.doi.org/10.1016/j.tafmec.2022.103496>.
- [60] NAUNHEIMER, Harald; BERTSCHE, Bernd; RYBORZ, Joachim; NOVAK, Wolfgang. **Automotive Transmissions: fundamentals, selection, design and application**. Springer, 2011. (ISBN: 978-3-642-16214-5). <https://link.springer.com/book/10.1007/978-3-642-16214-5>.
- [61] NENTWICH, Corbinian; DAUB, Rüdiger. Comparison of Data Sources for Robot Gear Condition Monitoring. **Procedia Cirp**, [S.L.], v. 107, p. 314-319, 2022. Elsevier BV. <http://dx.doi.org/10.1016/j.procir.2022.04.051>.
- [62] NING, Jieyu; CHEN, Zaigang; WANG, Yawen; LI, Yifan; ZHAI, Wanming. Vibration feature of spur gear transmission with non-uniform depth distribution of tooth root crack along tooth width. **Engineering Failure Analysis**, [S.L.], v. 129, p. 105713, Nov. 2021. Elsevier BV. <http://dx.doi.org/10.1016/j.engfailanal.2021.105713>.
- [63] NORTON, Robert L. **Machine Design: an integrated approach**. 6. ed. Pearson, 2021. (ISBN-13: 9780137516872). <https://www.pearson.com/store/p/machine-design-an-integrated-approach/P200000003435/9780137516872>.
- [64] OZEN, Emine Burcin; KORKMAZ, Yezdan Medet; COKER, Demirkan. Investigation of fretting fatigue failure mechanism of lug-bush connection members. **Procedia Structural Integrity**, [S.L.], v. 21, p. 215-223, 2019. Elsevier BV. <http://dx.doi.org/10.1016/j.prostr.2019.12.104>.
- [65] PALERMO, Antonio; BRITTE, Laurent; JANSSENS, Karl; MUNDO, Domenico; DESMET, Wim. The measurement of Gear Transmission Error as an NVH indicator: theoretical discussion and industrial application via low-cost digital encoders to an all-electric vehicle gearbox. **Mechanical Systems And Signal Processing**, [S.L.], v. 110, p. 368-389, Sep. 2018. Elsevier BV. <http://dx.doi.org/10.1016/j.ymssp.2018.03.005>.
- [66] PARMLEY, Robert O. **Illustrated Sourcebook of Mechanical Components**. McGraw-Hill Professional, 2000. (ISBN 13: 9780070486171). <https://www.mhprofessional.com/illustrated-sourcebook-of-mechanical-components-9780070486171-usa>.
- [67] PEI, Jiaying; HAN, Xu; TAO, Yourui; FENG, Shizhe. Lubrication reliability analysis of spur gear systems based on random dynamics. **Tribology International**, [S.L.], v. 153, p. 106606, Jan. 2021. Elsevier BV. <http://dx.doi.org/10.1016/j.triboint.2020.106606>.
- [68] PLEGUEZUELOS, Miguel; SÁNCHEZ, Miryam B.; PEDRERO, José I.. Control of transmission error of high contact ratio spur gears with symmetric profile modifications. **Mechanism And Machine Theory**, [S.L.], v. 149, p. 103839, Jul. 2020. Elsevier BV. <http://dx.doi.org/10.1016/j.mechmachtheory.2020.103839>.
- [69] QIN, W.J.; GUAN, C.y.. An investigation of contact stresses and crack initiation in spur gears based on finite element dynamics analysis. **International Journal Of Mechanical Sciences**, [S.L.], v. 83, p. 96-103, Jun. 2014. Elsevier BV. <http://dx.doi.org/10.1016/j.ijmecsci.2014.03.035>.
- [70] RAEYMAEKERS, Bart. **Design of Mechanical Elements: a concise introduction to mechanical design considerations and calculations**. Wiley, 2022. 256 p. (ISBN: 978-1-119-84996-4). <https://www.wiley.com/en-us/Design+of+Mechanical+Elements%3A+A+Concise+Introduction+to+Mechanical+Design+Considerations+and+Calculations-p-9781119849964>.
- [71] RAGHUWANSHI, Naresh K.; PAREY, Anand. Effect of Back-side Contact on Mesh Stiffness of Spur Gear Pair by Finite Element Method. **Procedia Engineering**, [S.L.], v. 173, p. 1538-1543, 2017. Elsevier BV. <http://dx.doi.org/10.1016/j.proeng.2016.12.239>.
- [72] REGIS, Amandine; ARROYAVE-TOBON, Santiago; LINARES, Jean-Marc; MERMOZ, Emmanuel. Physic-based vs data-based digital twins for bush bearing wear diagnostic. **Wear**, [S.L.], v. 526-527, p. 204888, Aug. 2023. Elsevier BV. <http://dx.doi.org/10.1016/j.wear.2023.204888>.
- [73] REJITH, R; KESAVAN, D.; CHAKRAVARTHY, P; MURTY, S.V.s. Narayana. Bearings for aerospace applications. **Tribology International**, [S.L.], v. 181, p. 108312, Mar. 2023. Elsevier BV. <http://dx.doi.org/10.1016/j.triboint.2023.108312>.
- [74] RODA-CASANOVA, Victor; SANCHEZ-MARIN, Francisco; MARTINEZ-CUENCA, Raul. Convective heat transfer modelling in dry-running polymer spur gears. **International Journal Of Mechanical Sciences**, [S.L.], v. 241, p. 107927, Mar. 2023. Elsevier BV. <http://dx.doi.org/10.1016/j.ijmecsci.2022.107927>.

- [75] SÁNCHEZ, Miryam B.; PLEGUEZUELOS, Miguel; PEDRERO, José I.. Calculation of tooth bending strength and surface durability of internal spur gear drives. **Mechanism And Machine Theory**, [S.L.], v. 95, p. 102-113, Jan. 2016. Elsevier BV. <http://dx.doi.org/10.1016/j.mechmachtheory.2015.09.001>.
- [76] SHU, Yiliang; YANG, Guangxue; LIU, Zhiming. Experimental study on fretting damage in the interference fit area of high-speed train wheels and axles based on specimen. **Engineering Failure Analysis**, [S.L.], v. 141, p. 106619, Nov. 2022. Elsevier BV. <http://dx.doi.org/10.1016/j.engfailanal.2022.106619>.
- [77] SINGH, Akant Kumar; SIDDHARTHA; YADAV, Sanjay. Investigations on noise emission from functionally graded materials based polymer spur gears. **Materials Today: Proceedings**, [S.L.], v. 64, p. 1496-1499, 2022. Elsevier BV. <http://dx.doi.org/10.1016/j.matpr.2022.04.970>.
- [78] SKAKOON, James G.. **The Elements of Mechanical Design**. New York: ASME, 2008. 104 p. (ISBN: 9780791802670). <https://www.asme.org/publications-submissions/books/find-book/elements-mechanical-design/print-book>.
- [79] SPECK, James A.. **Mechanical Fastening, Joining, and Assembly**. 2. ed. Oxfordshire, England, Uk: Routledge, 2015. 384 p. (ISBN 9781138748408). <https://www.routledge.com/Mechanical-Fastening-Joining-and-Assembly/Speck/p/book/9781138748408#>.
- [80] SUO, Haoyuan; WEI, Zhaohui; LUO, Bin; WANG, Linxuan; ZHANG, Kaifu; LIANG, Biao; DENG, Kelin; CHENG, Hui. Interfacial wear damage mechanism between Ti-alloy and Al-alloy in interference-fit joint and influence of surface coatings: experimental and numerical study. **Engineering Failure Analysis**, [S.L.], v. 143, p. 106931, Jan. 2023. Elsevier BV. <http://dx.doi.org/10.1016/j.engfailanal.2022.106931>.
- [81] VOINA, Andrei; BEREZHNOI, Sergei; YUNIN, Vladimir. Sprocket with asymmetric teeth for roller chain drives of vehicles. **Transportation Research Procedia**, [S.L.], v. 63, p. 1281-1287, 2022. Elsevier BV. <http://dx.doi.org/10.1016/j.trpro.2022.06.136>.
- [82] WITTEL, Herbert; MUHS, Dieter; JANNASCH, Dieter; VOßIEK, Joachim. **Roloff/Matek Maschinenelemente: normung, berechnung, gestaltung - lehrbuch und tabellenbuch**. Wiesbaden: Vieweg+Teubner Verlag Wiesbaden, 2011. 679 p. (EBook ISBN 978-3-8348-8279-0). <https://doi.org/10.1007/978-3-8348-8279-0>.
- [83] WOLLMANN, T.; NITSCHKE, S.; KLAUKE, T.; BEHNISCH, T.; EBERT, C.; FÜBEL, R.; MODLER, N.; GUDE, M.. Investigating the friction, wear and damage behaviour of plain bearing bushes of the variable stator vane system. **Tribology International**, [S.L.], v. 165, p. 107280, Jan. 2022. Elsevier BV. <http://dx.doi.org/10.1016/j.triboint.2021.107280>.
- [84] YAGHOUBI, Majid; TAVAKOLI, Hamed. **Mechanical Design of Machine Elements by Graphical Methods**. Springer, 2022. (ISBN: 978-3-031-04329-1). <https://link.springer.com/book/10.1007/978-3-031-04329-1>.
- [85] YAO, Yong; GUI, Gui; YANG, Suixian; ZHANG, Sen. An adaptive anti-noise network with recursive attention mechanism for gear fault diagnosis in real-industrial noise environment condition. **Measurement**, [S.L.], v. 186, p. 110169, Dec. 2021. Elsevier BV. <http://dx.doi.org/10.1016/j.measurement.2021.110169>.
- [86] ZHANG, Chao; CAO, Peng; ZHU, Rupeng; CHEN, Weifang; WANG, Dan. Dynamic modeling and analysis of the spline joint-flexible coupling-rotor system with misalignment. **Journal Of Sound And Vibration**, [S.L.], v. 554, p. 117696, Jun. 2023. Elsevier BV. <http://dx.doi.org/10.1016/j.jsv.2023.117696>.
- [87] ZHAO, Jiang; SHENG, Wei; LI, Zhengminqing; ZHANG, Hong; ZHU, Rupeng. Effect of lubricant selection on the wear characteristics of spur gear under oil-air mixed lubrication. **Tribology International**, [S.L.], v. 167, p. 107382, Mar. 2022. Elsevier BV. <http://dx.doi.org/10.1016/j.triboint.2021.107382>.
- [88] ZHOU, Yang; LI, Hongchao; WU, Genshang; SUN, Xinyao; LI, Dalei. Research on quality detection method for axis-hole interference fit based on laser ultrasound. **Measurement**, [S.L.], v. 185, p. 110051, Nov. 2021. Elsevier BV. <http://dx.doi.org/10.1016/j.measurement.2021.110051>.
- [89] ZHU, Xiang; DAI, Yu; MA, Feiyue. CFD modelling and numerical simulation on windage power loss of aeronautic high-speed spiral bevel gears. **Simulation Modelling Practice And Theory**, [S.L.], v. 103, p. 102080, Sep. 2020. Elsevier BV. <http://dx.doi.org/10.1016/j.simpat.2020.102080>.

APPENDIX A - DIDACTIC MATERIAL FOR MACHINE DESIGN COURSE

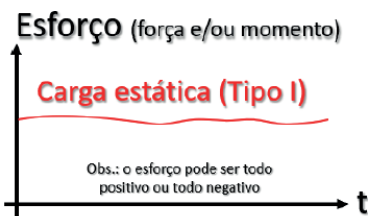
The main author of this article is a university professor at an Engineering college with extensive experience in the subject of Machine Elements. This discipline includes the specification of mechanical assemblies between cubes and shafts. One of the well-known techniques is interference fit, which is widely covered in reference books such as Shigley, Norton, Juvinall, Collins, among others. To facilitate his lectures, the professor has created a form that contains the most common mathematical expressions. All mathematical expressions are found in reference books. However, each book uses different terminology to describe each variable. The following figure presents the variables, their units, and the mathematical relationships.

Eixos ranhurados => Z: número de ranhuras. **L:** comprimento útil do contato com o cubo [mm]. **T:** torque [Nmm]

<p><i>Eixos entalhados</i> DIN 5462:1955-09; DIN 5463:1955-09; DIN 5471:1974; DIN 5472:1980</p> 	<p><i>Eixos dentados</i> DIN 5481:2019-04; DIN 5480-2:2015-03</p> 	<p>Em eixos ranhurados deve-se verificar apenas o critério do esmagamento. As dimensões são usadas em [mm].</p> <p>Esmagamento: $P_{atuante} \leq P_{adm}$</p> $\frac{T}{0,75 \cdot Z \cdot r \cdot L \cdot h} \leq P_{adm}$ $r = \frac{d_2 + d_1}{4} ; h = \frac{d_2 - d_1}{2}$
---	---	--

Observações=> chavetas temperadas e eixos ranhurados temperados: $1,5xP_{adm}$. 2 chavetas@120°: $L_{120^\circ} = \frac{2}{3} \cdot L_{calculado}$

Valores recomendados para p_{adm} em eixos de aço			
Fonte: Roloff e Matek (2011)			
Carregamento: choques x tipo de carga	Material do cubo	Chavetas côncavas de aço	Chavetas retangulares de aço, eixos ranhurados de aço
Choques fracos x Carga I ou II	Ferro fundido	40	60
	Aço	65	100
Choques fortes x Carga I ou II	Ferro fundido	25	40
	Aço	50	80
Choques fracos x Carga III	Ferro fundido	20	30
	Aço	33	50
Choques fortes x Carga III	Ferro fundido	13	20
	Aço	25	35



Unões por interferência

Dímetros [mm]: CUBO => D : nominal; D_e : externo; D_i : interno; eixo=> d : nominal; d_e : externo; d_i : interno.

p : pressão entre as peças (CUBO/eixo) em decorrência da interferência entre elas [MPa]. T : torque [Nm]; força axial F_a [N]. Índices usados nas fórmulas => i: peça interna; e: peça externa. Notação dos afastamentos => CUBO: LETRA MAIÚSCULA; eixo: letra minúscula.

Afastamentos [μm] => eixo: a_{min} ; a_{max} FURO: A_{min} ; A_{max} .

Interferências [μm] => Z : real (pós-montagem); I : inicial (pré-montagem); ΔI : perda de interferência na montagem. R_a : rugosidade superficial média [μm].

$$Z_{min} = I_{min} - \Delta I = a_{min} - A_{max} - \Delta I$$

$$Z_{max} = I_{max} - \Delta I = a_{max} - A_{min} - \Delta I$$

Obs.: a eventual perda de interferência (ΔI) depende do tipo de montagem.

Montagem axial forçada por prensagem com velocidade controlada ($\Delta I \neq 0$)

$$\Delta I = 1,2 \cdot (Ra_{CUBO} + Ra_{eixo})$$

$$F_m \geq 0,7 \cdot \pi \cdot 0,5 \cdot \mu \cdot k \cdot d \cdot L \cdot p_{max}$$

$$F_d \geq \pi \cdot \mu \cdot k \cdot d \cdot L \cdot p_{max} \quad ; \quad \mu_D = 0,5 \cdot \mu$$

Forças [N] => F_m : montagem; F_d : desmontagem
 μ : coeficiente de atrito estático [adimensional]
 μ_D : coeficiente de atrito dinâmico [adimensional]
 k : coeficiente de segurança para a fase de montagem ou desmontagem [adimensional]
 L : comprimento útil do contato no qual ocorre a interferência entre o CUBO e o eixo [mm]

Montagem radial por dilatação térmica ($\Delta I = 0$)

$$T_m = T_{amb} + \frac{I_{max} \cdot 10^{-3} + 5 \cdot 10^{-4} \cdot d}{\alpha \cdot d} \quad \Delta T = T_m - T_{amb}$$

Temperaturas [°C] => T_m : montagem; T_{amb} : ambiente; ΔT : variação de temperatura necessária para a montagem radial.
 d : diâmetro nominal [mm]; I_{max} : interferência máxima [μm]
 α : coeficiente de dilatação térmica [°C⁻¹]

Montagem	Prensagem axial				Dilatação radial			
	Eixo	Aço			Aço			
Cubo	Aço	FoFo	Alumínio	Latão	Aço	Aço	FoFo	Alumínio
Lubrificação	óleo	óleo	seco	seco	óleo	seco	seco	seco
μ	min.	0,05	0,07	0,02	0,03	0,08	0,07	0,07
	máx.	0,17	0,12	0,06	0,06	0,17	0,19	0,16

R_a [μm]	desbaste	médio	acabamento	
			fino	finíssimo
Simbologia	∇	∇∇	∇∇∇	∇∇∇
Classe ISO	N9-N10	N7-N8	N7-N8	N1↔N6
torneamento	16 a 40	x	6 a 16	3 a 6
fresamento	12 a 32	x	8 a 15	4 a 8
furação	10 a 25	6 a 10	3 a 6	x
retificação	16 a 40	6 a 16	3 a 6	1 a 3
brochamento	x	x	2 a 4	x

$$p_{min} = \frac{Z_{min} \cdot 10^{-3}}{(K_i + K_e) \cdot d_{eixo}}$$

$$p_{max} = \frac{Z_{max} \cdot 10^{-3}}{(K_i + K_e) \cdot d_{eixo}}$$

Pressão mínima entre CUBO e eixo [MPa]: p_{min}
 Pressão máxima entre CUBO e eixo [MPa]: p_{max}

Escorregamento: $f_{at} \geq R$

$$\pi \cdot \mu \cdot d \cdot L \cdot p_{min} \geq \sqrt{F_a^2 + \left(\frac{2 \cdot T}{d}\right)^2}$$

Forças [N] => f_{at} : atrito; R: resultante.
 Interferências reais [μ m]: Z (Z_{max} ou Z_{min}).

Esmagamento: $p_{atuante} \leq p_{adm}$

$$\text{eixo: } p_{max} \cdot \lambda_{(Q_i)} \leq \frac{\sigma_{e,eixo}}{n_{mec,eixo}}$$

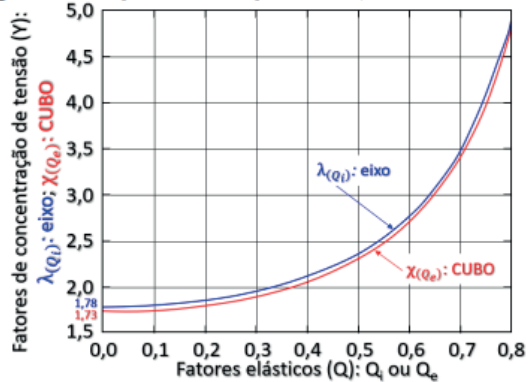
$$\text{CUBO: } p_{max} \cdot \chi_{(Q_e)} \leq \frac{\sigma_{e,CUBO}}{n_{mec,CUBO}}$$

$$K_i = \frac{1}{E_i} \cdot \left(\frac{1 + Q_i^2}{1 - Q_i^2} - \nu_i \right) ; Q_i = \frac{d_i}{d_e} ; K_e = \frac{1}{E_e} \cdot \left(\frac{1 + Q_e^2}{1 - Q_e^2} + \nu_e \right) ; Q_e = \frac{D_i}{D_e}$$

E: módulo de elasticidade axial [MPa]. ν : coeficiente de Poisson [adimensional].

Fatores elásticos [MPa^{-1}] => K_i : eixo; K_e : CUBO

Fatores geométricos [adimensional] => Q_i : eixo; Q_e : CUBO



Fatores de concentração de tensão $Y \Rightarrow \lambda_{(Q_i)}$: eixo; $\chi_{(Q_e)}$: CUBO

Coeficiente de segurança de esmagamento => n_{mec}

The professor maintains a YouTube channel where the courses he teaches are presented in playlists. During the lectures, the theory underlying the physical phenomena is explained, and all mathematical deductions are presented. For more information, please visit: https://www.youtube.com/channel/UCeRILnon_gofsbBvT3YDFPq

APPENDIX B - EXCEL SHEETS FOR CASE STUDY CALCULATIONS

The sheets include predefined formulas and built-in functions to handle complex calculations involved in determining parameters such as tooth strength, contact stress, bending fatigue, and power capacity. Additionally, they allow for easy customization and adaptation to specific design requirements and variations in gear system configurations.

The provided Excel sheets are accompanied by clear instructions and guidance on how to use them effectively. They enable engineers to quickly assess the power transmission capacity of spur gears mounted on shafts with spline bushes and make informed design decisions.

These Excel sheets serve as valuable supplementary material to the main content of the article, offering readers the opportunity to explore and apply the discussed methodologies in a practical and convenient manner. They can be accessed and utilized by interested individuals to gain a deeper understanding of the case study calculations or to apply the methods to their own gear system designs.

Please note that the Excel sheets are intended for educational and reference purposes and should be used in conjunction with proper engineering judgment and validation.

By providing Appendix B with the Excel sheets, readers will have access to practical tools that can enhance their understanding of the case study calculations and facilitate their own analysis and design processes.

In the spreadsheets presented below, the cells highlighted in yellow indicate data entries provided in the problem statement. This data is derived from the proposed questions. The cells in gray represent calculations performed using the input data, following the formulations provided in the reference materials. Lastly, the cells in red display the partial answers for each question.

Pressão admissível tabelada do contato entre CUBO e eixo entalhado	P_{adm}	20.00	[MPa]
Tem tratamento térmico no eixo entalhado?	Sim		
Pressão admissível do contato entre CUBO e eixo entalhado	P_{adm}	30.00	[MPa]
Número de entalhes do eixo entalhado	Z	8.00	[entalhes]
Diâmetro interno do eixo ranhurado	d_1	52.00	[mm]
Diâmetro externo do eixo ranhurado	d_2	60.00	[mm]
Braço da força de esmagamento	r	28.00	[mm]
Altura do entalhe	h	4.00	[mm]
Comprimento útil do contato entre o eixo ranhurado e o CUBO da engrenagem	L	35.00	[mm]
Torque máximo transmitido entre o eixo ranhurado e o CUBO da engrenagem	$T_{DIN 5463}$	705600.00	[Nmm]
a) Força de esmagamento que atua na face lateral dos entalhes	$F_{esm DIN 5463}$	4200.00	[Nmm]
Diâmetro nominal das peças montadas por interferência	$d=D$	40.00	[mm]
Afastamento máximo do CUBO	A_{max}	25.00	[μ m]
Afastamento mínimo do CUBO	A_{min}	0.00	[μ m]
Afastamento máximo do eixo	a_{max}	64.00	[μ m]
Afastamento mínimo do eixo	a_{min}	48.00	[μ m]
Interferência máxima teórica pré-montagem	l_{max}	64.00	[μ m]
Interferência mínima teórica pré-montagem	l_{min}	23.00	[μ m]
Tipo de montagem por interferência?	Radial, ou seja, $\Delta I=0$		
Perda de interferência	ΔI	0.00	[μ m]
Interferência máxima teórica pós-montagem	Z_{max}	64.00	[μ m]
Interferência mínima teórica pós-montagem	Z_{min}	23.00	[μ m]

Diâmetro interno do eixo	d_i	0.00	[mm]
Diâmetro externo do eixo	d_e	40.00	[mm]
Diâmetro interno do CUBO	D_i	40.00	[mm]
Diâmetro externo do CUBO	D_e	52.00	[mm]
Fator geométrico do eixo	Q_i	0.00	[adimensional]
Fator geométrico do CUBO	Q_e	0.77	[adimensional]
Módulo de elasticidade axial do material do eixo	E_i	109.00	[GPa]
Coefficiente de Poisson do material do eixo	ν_i	0.32	[adimensional]
Tensão limite de resistência ao escoamento do material do eixo	$\sigma_{e \text{ eixo}}$	56.00	[MPa]
Tensão limite de resistência à ruptura do material do eixo	$\sigma_{r \text{ eixo}}$	67.00	[MPa]
Módulo de elasticidade axial do material do CUBO	E_e	203.00	[GPa]
Coefficiente de Poisson do material do CUBO	ν_e	0.29	[adimensional]
Tensão limite de resistência ao escoamento do material do CUBO	$\sigma_{e \text{ CUBO}}$	240.00	[MPa]
Tensão limite de resistência à ruptura do material do CUBO	$\sigma_{r \text{ CUBO}}$	400.00	[MPa]
Fator elástico do eixo	K_i	6.239E-06	[MPa ⁻¹]
Fator elástico do CUBO	K_e	2.063E-05	[MPa ⁻¹]
Temperatura de operação do sistema	T_{amb}	32.00	[°C]
Coefficiente de dilatação linear do material estudado	α	-1.50E-05	[°C ⁻¹]
Temperatura de montagem por interferência radial	T_m	-108.00	[°C]
Variação de temperatura necessária para a montagem radial	ΔT	-140.00	[°C]
b) Variação de temperatura em módulo para a montagem radial	ΔT	-140.00	[°C]

Pressão mínima entre CUBO e eixo	p_{min}	21.40	[MPa]
Pressão máxima entre CUBO e eixo	p_{max}	59.54	[MPa]
Coefficiente de atrito dinâmico entre o eixo e a peça intermediária	μ_d	0.05	[adimensional]
Coefficiente de atrito estático entre o eixo e a peça intermediária	μ	0.10	[adimensional]
Coefficiente de segurança de desmontagem	k	1.80	[adimensional]
Comprimento útil do contato entre o eixo e a peça intermediária	L	60.00	[mm]
c) Força de desmontagem das peças montadas por interferência	F_d	80808.50	[N]
Fator de concentração de tensão do eixo	$\lambda_{(Q_i)}$	1.78	[adimensional]
Fator de concentração de tensão do CUBO	$\chi_{(Q_e)}$	4.23	[adimensional]
Coefficiente de segurança do eixo	$n_{mec \text{ eixo}}$	0.53	[adimensional]
d) Coeficiente de segurança do CUBO	$n_{mec \text{ CUBO}}$	0.95	[adimensional]
Força axial transmitida pela união por interferência	F_a	2750.00	[N]
Torque máximo transmitido pela união por interferência	T_{ajuste}	317950.88	[Nmm]
Torque máximo transmitido pela união (menor entre interferência e entalhes)	T_{ajuste}	317.95	[Nm]
Torque máximo transmitido pelas uniões	T_{ajuste}	0.32	[Nm]
Rotação do conjunto	n	300.00	[rpm]
Potência máxima transmitida pelas uniões	P	9988.72	[W]
e) Potência máxima transmitida pelas uniões	P	13.57	[CV]